The Lag3 and PD-1 pathways govern TCR signal duration and migration of CD4^{+} T cells

Lozan Sheriff[1], Alastair Copland[1], David A.J. Lecky[1], Reygn Done[1], Lorna S George[1], Emma K. Jennings[1#], Sophie Rouvray[1], Thomas A.E. Elliot[1], Elizabeth S. Jinks[1], Lalit Pallan[1] and David Bending[1*].

[1]Institute of Immunology and Immunotherapy, College of Medical and Dental Sciences, University of Birmingham, Birmingham B15 2TT, UK

[#]Current affiliation: Division of Biomedical Sciences, Warwick Medical School, University of Warwick, Coventry, UK

[*]Correspondence to d.a.bending@bham.ac.uk

Abstract

Anti-Lag3 and anti-PD-1 combination immunotherapy for melanoma has received recent regulatory approval, yet its mechanism of action is unclear, particularly for $CD4^+$ T cells. Here, we determined the roles of the Lag3 and PD-1/PD-L1 pathways during $CD4^+$ T cell activation *in vivo*. During primary immune responses, Lag3 played a redundant role with the PD1/PD-L1 axis dominant in regulating early $CD4^+$ T cell activation. By exploiting an adaptive tolerance model, we reveal that Lag3 and PD-L1 co-blockade (CB) drove major changes in $CD4^+$ T cells, resulting in a transcriptional profile dominated by a hybrid T follicular helper (Tfh)/Th17 cell phenotype. Mechanistically, CB enhanced T cell receptor (TCR) signal duration, thereby inducing an NFAT-biased transcriptional motif, previously linked to positive clinical outcomes for melanoma patients. Additionally, CB synergistically upregulated CCR6, leading to enhanced CCL20-mediated $CD4^+$ T cell migration. Analysis of melanoma patients on anti-PD-1 pathway immunotherapies revealed that tumour *CCR6* expression stratifies clinical outcomes and effector memory $CD4^+$ T cells upregulate *CCR6* in patients on anti-PD-1 and anti-Lag3 combination immunotherapy. Our data reveal that Lag3 and PD-1 pathways have context dependent roles in regulating the activation and migration of $CD4^+$ T cells and highlights *CCR6* as a biomarker for immunotherapy responses.

Introduction

Canonical T cell activation is initiated by the binding of the T cell receptor (TCR) to peptide-loaded major histocompatibility complexes (MHC). The integration of signals from co-stimulatory and co-inhibitory molecules fine-tunes this process(1) and can alter the threshold for T cell activation(2). Understanding how T cell activation thresholds are modulated has fundamental implications for the treatment of T cell-mediated diseases and the exploitation of T cell-modulating immunotherapies.

The immune checkpoints programmed cell death protein 1 (PD-1), cytotoxic T lymphocyte antigen 4 (CTLA-4) and lymphocyte activation gene 3 (Lag3), have been identified as critical regulators of T cell activation(3-5). All three molecules (and for PD-1 also its ligand PD-L1(6)), are current targets for immunotherapy(7, 8). Each of these checkpoints is thought to exhibit distinct functions on T cells. PD-1 contains immunoreceptor tyrosine-based inhibitory motifs (ITIMs) that allow it to recruit Src homology-2 domain-containing protein tyrosine phosphatase-2 (SHP-2)(9) phosphatases to target the TCR(10) and CD28(11). CTLA-4 acts on the CD28 pathway, and competes with CD28 for binding to the costimulatory molecules CD80/ CD86(12-14) and therefore regulates T cell co-stimulation(15). Lag3, a CD4 structural homologue(16), binds MHC class II(17) and is an important regulator of T cell activation and expansion(5). Indeed, increasing evidence highlights the importance of $CD4^+$ T cell tumour surveillance and control through recognition on peptide MHC II complexes(18). In addition, CD4 T cells are also essential for shaping and enhancing the anti-tumour cytotoxic CD8 response(19, 20).

An emerging paradigm is that the targeting of more than one immune checkpoint can lead to superior clinical outcomes(21). This has been observed first-hand in the clinic: combination therapy of Ipilimumab (anti-CTLA-4) and Nivolumab (anti-PD1) offers better patient survival compared to monotherapy in melanoma(7). Similarly, a recent study demonstrated superior progression-free survival (PFS) in patients on a combination therapy of Relatlimab (anti-Lag3) with Nivolumab(8). Although cross-trial comparisons are challenging, there is evidence that grade 3/4 adverse effects may be lower with Relatlimab plus Nivolumab combination therapy (21.1% combination therapy vs 11.1% in Nivolumab monotherapy(22)) compared to those observed in Ipilimumab plus Nivolumab (59% combination therapy vs 22% in Nivolumab monotherapy(23)). Nivolumab and Relatlimab were approved for use as a combination therapy for unresectable advanced melanoma in 2022 by the FDA and EMA, and in 2024 by NICE in the UK. Given that significant proportions of patients fail to respond to monotherapy(8, 23), a combination therapy with enhanced efficacy and more tolerable side effects is highly desirable. However, our understanding of how immune checkpoints fundamentally interact to regulate different $CD4^+$ T cell subsets is unclear.

We recently developed an accelerated adaptive tolerance model that can evaluate the effects of immune checkpoints on $CD4^+$ T cell activation *in vivo*(2, 24). Using this model, we showed that PD-1 acts as a rheostat to control the threshold for T cell activation. Its blockade leads to an enhanced TCR signal strength and the upregulation of co-stimulatory molecules, such as ICOS and OX40(2). Importantly, we found that the co-inhibitory receptor Lag3 was strongly up-regulated in these

tolerogenic CD4 T cells, and so we questioned what effect this pathway would have on T cell function in the context of PD-1 pathway blockade.

To investigate how Lag3 may regulate $CD4^+$ T cells in the context of PD-1 pathway blockade, we exploited the Tg4 TCR transgenic model, which is specific for myelin basic protein (MBP) peptide. MBP contains a lysine (K) at position 4, which exhibits unstable MHC binding to the $I\text{-}A^U$ class II molecule(25, 26). Substituting for a tyrosine (Y) generates an affinity for $I\text{-}A^U$ which leads to highly stable peptide/MHC II complexes(25, 27) which is potently recognised by the Tg4 transgenic TCR. Given that Lag3 has a preferential function for targeting stable peptide/MHC II complexes(28, 29) we were interested to further understand its role in the context of PD-1/PD-L1 pathway blockade during longer periods of immune activation with [4Y]-MBP.

In this study, we demonstrate that Lag3 and PD-L1 cumulatively govern $CD4^+$ T cell activation by increasing the duration of TCR signalling. This leads to an enhanced state of T cell activation, bolstered migration, and a T follicular helper (Tfh)/Th17 cell-biased phenotype. Finally, we show that these same signatures of extended TCR signalling duration and CCR6-associated migration can be found in melanoma patients receiving PD-1 incorporating immunotherapies, thus revealing new insights into fundamental CD4 T cell biology, while also unveiling new biomarkers for immunotherapy.

Results

PD-1 pathway is dominant over Lag3 in controlling initial CD4$^+$ T cell activation

To investigate the functions of the PD-1 and Lag3 pathways during a primary response we employed two different models for CD4$^+$ T cell activation. In all the following studies we used anti-PD-L1 to modulate the PD-1 pathway as we were interested in identifying T cell sub-populations expressing this marker. Firstly, Tg4 Nur77-Tempo mice were immunised with [4Y]-MBP peptide and we examined the ability of PD-L1, Lag3 or combination blockade (CB) to sustain TCR signalling during initial activation *in vivo* (**Figure 1A-E**). Nur77-Tempo mice report distal TCR signalling through expression of Fluorescent Timer(30) protein (FT), which has an initial Blue fluorescent form with a half-life of 4 hours before maturation to an irreversible Red fluorescent form. T cells that sustain TCR signalling during the first few days will appear as Blue$^+$Red$^+$ cells at the analysis time point (**Figure 1B**). Our experiments showed that only anti-PD-L1 treated or CB-treated mice showed significantly increased populations of CD4$^+$ T cell with persistent TCR signalling, with no noticeable effect of anti-Lag3 treatment alone (**Figure 1C**). In addition, we examined expression of ICOS, a marker linked to strong TCR signalling in response to anti-PD-1 treatment of re-activated CD4$^+$ T cells(2). In this setting we saw a significant upregulation of ICOS in the CB-treated mice compared to the other conditions (**Figure 1D**).

Next, to understand the roles of PD-L1 and Lag3 during a polyclonal immune response we utilised an immunisation approach with the model antigen NP-Ova (**Figure 1E**). Mice were immunised with NP-Ova precipitated in alum. Twenty-four hours later mice received either IgG, anti-PD-L1, anti-Lag3 or combination and 7

days later (day 8 post-immunisation) the popliteal lymph nodes were isolated and $CD4^+$ T cells analysed (**Figure 1F-H**). Anti-PD-L1 and CB significantly increased the frequency of Tfh cells compared to isotype and anti-Lag3 groups, but there was no additive effect of CB compared to anti-PD-L1 alone (**Figure 1G**). Analysis of ICOS levels on $CD4^+$ T cells (**Figure 1H**) revealed that, as with the previous Tg4 Nur77-Tempo model, CB imparted a significant increase in ICOS levels on $CD4^+$ T cells. In summary during early $CD4^+$ T cell activation, whilst the PD-L1/PD-1 pathway is dominant over Lag3 in regulating the process CB led to more consistent $CD4^+$ T cell activation in vivo.

Lag3 and PD-L1 pathways exert additive and synergistic effects on $CD4^+$ T cell activation during secondary stimulation

To further investigate the effects of co-blockade (CB) of Lag3 and PD-L1 *in vivo*, we therefore utilised our accelerated adaptive tolerance model(2, 24) to test CB potency effects following T cell reactivation (**Figure 2A**). In this model, a single high dose of [4Y]-MBP induces transient TCR signalling *in vivo* and upregulation of multiple immune checkpoints, including PD-1 and Lag3, thereby allowing an assessment of their functions (2). A secondary immunisation subsequently allows a dissection of the roles that Lag3 and PD-L1 play in the activation thresholds for $CD4^+$ T cells. CB significantly enhanced Nr4a3-Red^+Nr4a3-$Blue^+$ (i.e. cells that have persistent activity of the NFAT-*Nr4a3* pathway(31) and henceforth referred to as “responder” cells; mean = 33.3%) compared to isotype control (mean=7.9%) and single agent anti-PD-L1 (mean=21.7%) or anti-Lag3 (mean=18.5%) treatment (**Figure 2B and 2C**). We have previously identified ICOS and OX40 as markers of PD-1 response in $CD4^+$ T cells(2), so we were interested to further understand their regulation in the context of

CB. Analysis of ICOS and OX40 expression within responder cells (to normalise for differences in the frequency of T cell activation *in vivo,* **Supplementary Figure 1)** revealed a strikingly large increase in $CD4^+$ T cell surface expression of ICOS and OX40 in CB-recipient mice compared to IgG or single agent-treated mice (**Figure 2D**). We generated a surface protein metric called surface TCR.strong based on the geometric mean of OX40 and ICOS MFI (**Supplementary Figure 1)**, the transcripts of which we have previously reported to be enriched in melanoma patient responders to Nivolumab(2). Analysis of surface TCR.strong expression suggested that CB was exerting synergistic effects on the levels of OX40 and ICOS compared to individual treatments (**Figure 2E**). To further explore the effects of Lag3 and PD-L1 CB on responder and surface TCR.strong metrics, we performed statistical testing to determine whether any interaction (i.e. potential synergy) existed between the treatments (**Figure 2F**). The effect of combination therapy was additive for the responder population (parallel lines, p value for interaction=0.865, ns); however, for the surface TCR.strong metric a significant interaction was detected, highlighting a synergistic effect on ICOS and OX40 expression. As the analysis was performed on only responder populations, this effect is not driven by differential activation states in response to the different treatment regimes. These findings were also detected at a later time point (18hrs) post-secondary stimulation (**Figure 2G**). In summary, these data reveal that CB of Lag3 and PD-L1 drives additive increases in the proportion of CD4+ T cells that re-activate as well as synergistic increases in markers linked to strong TCR signalling in vivo.

Transcriptional analysis reveals Th17/Tfh cell bias and activation of an NFAT-biased gene signature in response to Lag3 and PD-L1 blockade

To gain an unbiased overview of phenotypic changes in $CD4^+$ T cells in response to CB, we repeated the experiments performed in Figure 2 but this time used FACS to isolate responder cell populations before performing 3' mRNA sequencing (**Figure 3A and 3B**). Isolating the responders alone (i.e. Timer+ cells) allowed us to normalise for different levels of activation between groups and to home-in on the qualitative changes induced by these treatments. Principal component analysis (PCA) showed that the treatments were largely separated by PC1, with CB-recipient mice the most distant from isotype and anti-Lag3 and anti-PD-L1-treated mice clustering close together (**Figure 3C**). Analysis of DEGs revealed that Lag3 and PD-L1 co-regulated genes associated with strong TCR signalling (*Icos, Tnfrsf4, Il21, Tnfrsf9, Maf, Irf8*(2)) but the DEG showing the highest log fold-change was the chemokine receptor *Ccr6* (**Supplementary Table 1**, **Figure 3D**). In addition, there were notable upregulated genes involved in glycolysis/metabolism (*Aldoa, Hk2, Hif1a*), NF-kB regulator gene *Bcl3,* and genes involved in ribosome biogenesis (*Gnl3, Wdr43*). Downregulated genes included the Th2-associated *Gata3,* as well as integrins *Itga4, Itga6* and also genes involved in lymphoid tissue retention (*Sell*, *S1pr1*) (**Figure 3E**). As we have observed previously(2) in strongly signalling $CD4^+$ T cells, genes encoding molecules involved in TCR signalling were also downregulated (*Cd4, Rasgrp2*). Having noticed a reduction in Gata3 (Th2 master transcription factor), we curated an analysis of genes associated with different T helper subsets (**Figure 3F**). Visualisation revealed a clear footprint for Tfh cells (notable differences for *Il21, Icos,* and *Maf*) and Th17-associated markers (although *Il17a* and *Il17f* transcripts were not detectable), including *Ccr6* which was also elevated in anti-PD-L1 treated mice (**Figure 3F**). Th1-, Th2- and Treg-associated transcripts were less

pronounced after CB treatment, albeit with clear variation in expression, reflecting low transcript abundance for many of these genes.

Given that *Nr4a3* is a direct NFAT target(31), we wanted to further understand whether the DEGs identified showed any relationship to NFAT signalling pathways. A recent study determined that 1089 genes in T cells are directly regulated by NFAT and ERK pathways during the first 30 hrs(32) – a similar time frame to our in vivo studies. Through incorporation of inhibitors of NFAT or ERK pathways, Wither et al. determined the relative dependence of genes on these signalling axes. We intersected the 189 genes that were upregulated in $CD4^+$ T cell responders between CB-treated and isotype-treated mice with the 1089 identified in Wither et al. Thirty-nine genes were found to overlap between the two data sets (**Figure 3G**). The expression of these genes was then visualised across the four treatment groups from RNA-seq data (**Figure 3H**), with additional annotation based on the dependence of ERK and/or NFAT pathways as defined in Wither et al(32). The vast majority of the genes (33 out of 39) were associated with co-operative ERK/NFAT signalling, but with an NFAT-biased signature, implying a stronger contribution to their regulation from the NFAT pathway compared to ERK. Included in these groups were *Tnfrsf4* (OX40), *Icos* and *Irf8* which exhibited co-operative regulation (with NFAT bias), highlighted by red arrows. We confirmed the binding of NFAT1 to the genes encoding Nr4a3, ICOS, IRF8 and OX40 (**Supplementary Figure 2**) in publicly available datasets from murine T cells(33). All four genes displayed sharp NFAT1 binding peaks that were evident 0-10kb upstream from the transcription start sites of each gene, highlighting a link to TCR-NFAT signalling in driving their sustained expression. Taken together, CB imparts a novel transcriptional signature on $CD4^+$ T

cells undergoing reactivation *in vivo*, exhibiting hallmarks of NFAT-biased TCR signalling, metabolic priming and a T follicular helper cell bias.

Combination blockade biases towards Tfh cell development and synergistically upregulates CCR6

Our transcriptional analysis showed that CB imparts a Tfh-like phenotype in $CD4^+$ T cells. Tfh cells are known to possess a signature of genes activated downstream of the TCR (including metabolic, cell cycle and cytokine genes(34)) and are sustained by AP-1-independent NFAT signals(35) (i.e. NFAT-biased signalling). Therefore, we sought to validate that PD-L1 and Lag3 enhanced Tfh cell differentiation *in vivo* during $CD4^+$ T cell reactivation (**Figure 4A**). We employed our accelerated adaptive tolerance model and analysed $CD4^+$ T cells for markers of Tfh cell development: PD-1, CXCR5 and ICOS (**Figure 4B**). As can be seen, CB drove enhanced differentiation of Tfh cells (**Figure 4C**) compared to all other treatment conditions, and these cells expressed significantly elevated levels of ICOS at both the bulk $CD4^+$ T cell level (**Figure 4D**) as well as within the Tfh subset (**Figure 4E**) compared to all other treatment groups.

Since transcriptional analysis by RNA-seq provides only a 'snapshot-in-time' view, we wanted to analyse protein levels of the other notable markers identified previously. We performed an identical experiment as in Figure 2A and then evaluated protein intracellular levels of IRF8 (a DEG and part of the TCR.strong metric(2)) and IRF4 (previously linked in this model to strong TCR signalling(2)) (**Figure 4F and 4G**). Analysis revealed that CB increased levels of IRF8 compared to all three treatment groups, whilst for IRF4 CB increased the levels compared to

control and anti-PD-L1 treated mice. In addition, we validated whether the upregulation of *Ccr6* also occurred at the protein level. Analysis of surface CCR6 revealed a sharp, synergistic upregulation (more than 30% of cells now positive for this marker) in response to CB (**Figure 4H and 4I**). In sum, protein validation of the RNA-seq revealed that CB enhanced Tfh-like cell development and increased surface CCR6 protein levels.

PD-L1 and Lag3 co-operatively regulate TCR signal duration in CD4$^+$ T cells

The maturation of Timer Blue proteins into Timer Red can give an estimation of the signal duration within an actively signalling T cell population (**Figure 5A**). This is because TCR signalling triggers new formation of Timer Blue proteins, which have a half-life of four hours, before maturation into the longer lived Red proteins from (half-life of 3-5 days). A short TCR signal will thus lead to an increase and then fall in Red proteins, whilst sustained signalling will lead to accumulation of mature Timer Red proteins. We hypothesised that the enhanced NFAT-biased signature observed is a result of CB sustaining TCR signalling for a longer period following reactivation *in vivo* and we therefore re-analysed the levels of Timer Red protein within “responder” cells from Figure 2F and 2G across the four treatment groups. Analysis at 12 hrs post-reactivation in the presence of CB showed a small but significant accumulation of Timer Red proteins compared to the three other groups, however a small increase in Timer Red was also observed in the anti-PD-L1 treated mice (**Figure 5B**). Analysis at the later 18 hr timepoint revealed that only CB exhibited a significant increase in Timer Red, which demonstrates that these cells have signalled for a longer period (**Figure 5C**).

We next wanted to test whether key markers identified in Figure 3 were regulated by the duration of TCR signalling. Given the challenges of inhibiting TCR signalling *in vivo*, we established a new *in vitro* model to assess the relative contributions of the PD-L1 and Lag3 pathways controlling *in vitro* TCR signal strength in adaptively tolerised T cells (**Supplementary Figure 3**). Splenocytes from Tg4 *Nr4a3*-Tocky *Il10*-GFP mice were isolated 24 hrs after *in vivo* immunisation and cultured in the presence of IgG isotype control, anti-PD-L1, anti-Lag3 or combination in the presence of a dose titration of [4Y]-MBP (**Supplementary Figure 3A**). To demonstrate that this model can reveal manipulations into TCR signal strength, we evaluated ICOS and OX40 expression on $CD4^+$ Nr4a3-Red^+ Nr4a3-$Blue^+$ T cells. Using 'surface' TCR.strong metric based on the geometric mean of surface ICOS and OX40 expression we could see that the model faithfully captured alterations in TCR signal strength (**Supplementary Figure 3B**) since CB of Lag3 and PD-L1 augmented TCR signal strength across a dynamic range of peptide concentrations. Next, to address how TCR signal duration influences expression of the key markers ICOS, OX40, IRF8 and *Nr4a3* we cultured antigen-adapted Tg4 T cells *in vitro* in the presence of [4Y]-MBP and added the Src kinase inhibitor PP2 to terminate TCR signalling after 0, 4, 8, 12 or 24 hours (**Figure 5D**). Cells remained in culture for the full 24 hours before analysis of Nr4a3-Blue, ICOS, OX40 and IRF8 expression. As expected, Nr4a3-Blue expression continued to increase in parallel with the increase in TCR signal duration (**Figure 5E**). ICOS expression showed a delayed response but rose prominently from 4 hrs to 12 hrs with a gradual increase up to 24 hrs (**Figure 5E**). IRF8 showed a similar pattern but its induction required longer periods of TCR signalling (minimum of 12 hrs), and gradually increased thereafter (**Figure 5E**). OX40 showed a time dependent increase from the initiation of TCR signalling

but plateaued from 12 to 24 hrs (**Figure 5E**). Thus, CB results in an increased duration of TCR signalling, which accounts for the time-dependent and synergistic upregulation of ICOS, IRF8 and OX40.

Elevated tumour *CCR6* expression associates with enhanced survival in melanoma patients on PD-1 pathway targeting immunotherapies

We have previously shown that ICOS, IRF8 and OX40 gene expression is linked to successful outcomes to PD-1 pathway immunotherapy in melanoma patients(2). Given the stark increase in CCR6 in anti-PD-L1+anti-Lag3-treated mice we investigated whether CCR6 expression is clinically relevant in the context of PD-1 pathway immunotherapy through analysis of RNA-seq datasets of patient tumour biopsies taken before and after anti-PD-1. Analysis of the Riaz et al.(36) cohort revealed that pre-therapy, tumour *CCR6* expression showed no significant association with clinical outcomes (**Figure 6A**). However, on-therapy tumour biopsies showed significantly higher *CCR6* expression in patients that showed treatment benefit (**Figure 6B**). Furthermore stratifying the Riaz cohort by previous Ipilimumab status revealed that those who were ipilimumab naïve (i.e. only received anti-PD-1 with no prior anti-CTLA-4 treatment) had significantly increased overall survival when patients were stratified by *CCR6* expression levels within their on-therapy tumour biopsies (**Figure 6C-D**). In addition *CCR6* transcripts showed a significant positive correlation with *CCL20*, the ligand for CCR6, within the on-therapy tumour biopsies (**Figure 6E**). The findings regarding tumour CCR6 expression was replicated in a separate patient cohort of early during treatment biopsies of melanoma patients on PD-1/PD-L1 immunotherapy from the Gide et al.(37) cohort (**Figure 6F**). Combining the datasets from both the Gide and Riaz

studies (where both datasets were classified as high or low based on each cohorts respective median expression and then pooled) revealed that high tumour *CCR6* expression in on-therapy tumour biopsies significantly associated with increased overall survival (**Figure 6G**).

CCR6 upregulation in human effector memory CD4$^+$ T cells on Nivolumab and Relatlimab combination therapy

A recent study provided insight into transcriptional changes occurring on therapy in peripheral blood T cells in patients receiving anti-PD-1 and anti-Lag3 combination therapy (specifically Relatlimab and Nivolumab(38)). We investigated whether transcriptional changes identified in our murine models were also reflected in this cohort of human patients on combination therapy. We selected DEGs in human CD4 naive/central memory (CM), human CD4 effector memory (EM)/Th1 and human Treg and intersected these with DEGs identified between combination therapy treated murine CD4s and controls (**Figure 7A-C**). Upregulated across all 4 conditions was the NF-kB regulator gene *BCL3/Bcl3*, which has also been linked to inhibiting Treg development and function(39). Interestingly, *ICOS* showed upregulation across human CD4 naïve/CM and EM/Th1 cells. In addition consistent with our observation in the Riaz(36) and Gide(37) cohorts, *CCR6* was upregulated within human effector memory/Th1 subsets.

In human Treg, the gene encoding OX40 (*TNFRSF4)* was also notably upregulated, along with RRS1 (ribosome biogenesis; a pathway noted in our murine RNAseq), *ISG15* (involved in type I IFN signalling) and *TENT5C* (mRNA stabilisation and NFAT driven). Notable downregulated genes in all 4 subsets included *GATA3* (Th2) and

TRAF3IP3 (required for Treg maintenance and function(40)). Human CD4 Treg and human CD4 effector memory cells also showed downregulation of *DGKA* and *SIT1* (involved in TCR signalling). Notable other genes downregulated in human CD4 T EM/Th1 group also included *CORO1A (*which has roles in regulating allograft tolerance) *CDC25B* (cell cycle regulation) and *ANXA6* (involved in IL-2 sensing(41)) and *RAC2* (deficiency of which affects T cell activation(42)), and *ITGA4* (linked in mice to Th1 cell homing)(43). These findings confirm that peripheral human $CD4^+$ T cells accurately reflect the murine *in vivo* phenomena and highlight ICOS, CCR6 and OX40 as clinical relevant biomarkers for treatment monitoring.

Finally, given the link between CCR6 expression levels and immunotherapy outcomes, we investigated the migratory capacity of FACS-purified $CD4^+$ T cells following in vivo CB using a migration assay (**Figure 7D**). In response to CCL20, $CD4^+$ T cells from CB-treated mice showed significantly enhanced migration towards CCL20, highlighting that PD-1 incorporating immunotherapies can enhance CCR6-dependent migration of $CD4^+$ T cells.

Discussion

Our study demonstrates that the PD-L1 and Lag3 pathways exert non-redundant control on the duration of TCR signalling in $CD4^+$ T cells. PD-1 itself can directly target the TCR(10) and CD28(11) molecules, which allows PD-1 to act as a rheostat to control TCR signal strength(2). PD-1 contains tyrosine-based motifs (ITIM and ITSM(44)) that allow recruitment of SHP-2 phosphatases that mediate its inhibitory function(9). Lag3 on the other hand has proven more enigmatic in its function. Whilst its binding to MHC Class II is well established(28, 29), Lag3 also has other reported ligands of relevance to T cell biology: galectin-3(45), fibrinogen-like protein 1 (FLP-1)(46) and the TCR-CD3 complex(47). Whilst stable peptide MHC Class II appear more important than FLP-1 for T cell inhibition *in vitro*, the hierarchy of ligands *in vivo* remains unclear(48). Our findings show that Lag3 works co-operatively with the PD-1/PD-L1 pathway to regulate the T cell activation threshold of $CD4^+$ T cells *in vivo*. Mechanistically, co-blockade of PD-L1 and Lag3 results in an increased duration of TCR signalling, which drove synergistic increases in the TCR signal duration-dependent receptors OX40, ICOS.

Interestingly, the effect of Lag3 blockade alone was generally weaker than the PD-L1 pathway *in vivo*, which Vignali and colleagues have also previously noted(47). In addition, Lag3 had minor effects on the primary CD4+ T cell response and its major effects were only exerted in the presence of PD-1 pathway blockade. These findings may be due to broader T cell PD-1 expression and the susceptibility of Lag3 to ADAM-mediated shedding(49). Indeed, ADAM-resistant forms of Lag3 confer resistance to anti-PD-1 immunotherapy *in vivo(50)*, which is linked to reduced $CD4^+$ T cell help for $CD8^+$ T cells. It is possible that PD-1 blockade itself may augment the

ability of Lag3 to interact with its potential ligands (e.g., MHC class II), which could result in an increased potency of Lag3 in our model, particularly as [4Y]-MBP peptide generates highly stable peptide-MHC II complexes. Given that in the immunised setting blockade of Lag3 resulted in much weaker effects than in the adaptive tolerance conditions, this may reflect the higher levels of Lag3 that are induced on the tolerised $CD4^+$ Tg4 T cells.

The fact that PD-1 pathway appears more potent than Lag3 could also reflect hierarchical levels of T cell tolerance, whereby upon loss of the PD-1 pathway, Lag3 plays a much greater functional role. It is also likely that blockade of the PD-1 pathway may alter the dwell times of T cells on APCs *in vivo*. Tolerised islet antigen-specific T cells showed enhanced motility when scanning DCs in pancreatic draining lymph node(51). Blockade of PD-L1 or PD-1 led to reduced T cell motility and precipitation of autoimmune diabetes; however blockade of CTLA-4 had no effect on T cell motility(51) despite past reports that CTLA-4 may limit formation of stable APC:T cell conjugates(52).

A previous study demonstrated functional synergy of PD-1 and Lag3 in the control of anti-tumour immunity(53), and this was linked to increases in IFNγ-expressing cells amongst both $CD4^+$ and $CD8^+$ T cells(53). Unlike $CD8^+$ T cells, $CD4^+$ T cells have less clearly defined roles in tumour development, exerting anti-tumour effects through effector cytokines, cytotoxicity, and T cell help (reviewed in(54)). However, evidence for pro-tumour development comes from the association of $CD4^+$ $Foxp3^+$ Tregs with poor clinical outcomes(55). Nonetheless, expansion of Tfh cells in human tumours has been observed following anti-PD-1 immunotherapy(56). In solid

tumours, Tfh cells likely have a beneficial role(57) and their tumour infiltration is positively correlated with clinical outcome in human breast cancer(58). Mechanistically, Tfh cell-derived IL-21 was linked to enhancing $CD8^+$ T cell function in mouse models of lung adenocarcinoma(59).

It is possible that the Tfh cell correlation with clinical outcomes in cancer may reflect neoantigen release which may promote their differentiation and execution of anti-tumour immune functions. However, in the context of immunotherapy, Tfh cell differentiation has been shown to be notably altered(57). A study assessing cancer-irrelevant immune responses to seasonal flu vaccination describe an increased Tfh cell response in patients on anti-PD-1 therapy(60). Tfh cell signatures are positively correlated with immune related adverse events (irAEs) in humans(61). Interestingly, similar findings have been observed in murine studies using aged mice (18-24 months), which showed the development of IgG-mediated disease that was linked to an IL-21-producing Tfh-like subset(62). In the present study, combination treatment robustly drove enhanced Tfh cell development, but its most notable effect was the induction of higher ICOS expression. Given that ICOS is an essential costimulatory molecule for Tfh cell responses *in vivo*(63) it will be important to understand its wider potential effects on humoral immunity.

The potential manipulation of Tfh cell biology by checkpoint blockade comes with inherent risk. Genetic analysis of SNPs have linked a variant (rs17388568) associated with increased risk of ulcerative colitis(64) and type 1 diabetes(65) with an enhanced response to anti-PD-1 in metastatic melanoma patients(66). The risk variant maps to a genomic region containing *IL2* and *IL21*, which are critical

cytokines involved in regulation of $CD4^+$ and Tfh cell responses. Future work should address the extent to which Tfh cell development is altered in patients on immune therapies targeting PD-1 and/ or Lag3 pathways and how these relate to irAEs.

Upregulation of CCR6 was a clear feature of $CD4^+$ T cells restimulated in the presence of antibodies to PD-L1 and Lag3 – a finding also seen in analysis of single-cell RNAseq data of human $CD4^+$ effector memory subsets in peripheral blood(38). CCR6 has been identified as a marker of autoreactive but tolerogenic CD4 memory T cells in vivo(67). Interestingly, IL-21 has been shown to be the major factor that leads to CCR6 upregulation on T cells in culture(68). The CCL20/CCR6 axis has been heavily implicated in the metastasis of cancer cells(69) but CCR6 is also being exploited as a tumour-homing chemokine in the Chimeric Antigen Receptor (CAR) T cell field(70). Our findings that PD-1 and Lag3 pathway blockade can alter T cell migratory properties is therefore important and warrants further investigation.

In addition to CCR6, we also observed changes to the integrins *Itga4* and *Itga6* and downregulation of L-selection (encoded by *Sell*). Therefore, CB of Lag3 and PD-L1 promotes an effector/ migratory CD4+ T cell phenotype. Whilst CCR6 is associated with Th17 cells(71), it is also associated with antigen-experienced memory T cells in humans(72), and subsets of so-called “circulating” Tfh cells in humans(73). The CCR6:CCL20 axis in mice has been shown to be pivotal to Th17 cell-mediated autoimmune arthritis in mice(74). This axis has also been linked to the recruitment of T cells into inflammatory tissues(75). Therefore, upregulation of CCR6 may enhance the recruitment of T cells to inflamed sites. However, recent work addressing correlates of toxicity to immunotherapy has highlighted that pre-existing abundance

of activated $CD4^+$ memory T cells and TCR diversity are significantly associated with irAEs in melanoma(76). Recent data from the RELATIVITY-047 phase 2/3 clinical study, which demonstrated that Relatlimab (human IgG4-Lag3 blocking antibody) in combination with Nivolumab showed superior progression free survival(8). Nonetheless, combination therapy was associated with an increased level of grade 3/4 treatment related adverse events (21.1 vs 11.1%)(22). It will be imperative to further explore potential mediators of these irAEs in combination therapy-treated patients in the future. Identification of potential biomarkers for treatment monitoring in this study may aid in further understanding the correlates of treatment efficacy as well as their relationship to irAEs.

A recent study suggested that the ligand-dependent suppression by Lag3 depended on its cytoplasmic RRFSALE motif(77). Intriguingly, this study also showed that blocking Lag3 can enhance T cell activation even in the absence of ligands for Lag3 *in vitro*(77). Given that PD-1 can exhibit tonic signalling which drives a basal level of suppression(78), it will be interesting to determine whether the mere expression of Lag3 is also in itself sufficient to mediate some of its inhibitory functions in $CD4^+$ T cells.

In summary, our study provides new insight into how the PD-1 and Lag3 pathways intersect to govern multiple aspects of $CD4^+$ T cell activation *in vivo* and identifies CCR6 as a clinically meaningful readout for PD-1 incorporating immunotherapies.

Methods

Mice

Nr4a3-Tocky(79) lines were modified by mating to Tg4 *Il10*-GFP mice as previously described(80) to generate Tg4 *Nr4a3*-Tocky *Il10*-GFP mice(31) (unmodified Nr4a3-Tocky lines were originally obtained from Dr Masahiro Ono (Imperial College London) under MTA; the manuscript does not report any findings arising from the use of unmodified *Nr4a3*-Tocky lines or modified *Nr4a3*-Tocky lines that have not been previously reported in the literature. Nur77-Tempo mice(81) were mated to Tg4 *Il10*-GFP mice to generate Tg4 Nur77-Tempo mice. C57BL/6J mice were purchased from Charles River. All animal experiments were approved by the local animal welfare and ethical review body and authorised under the authority of Home Office licenses P18A892E0A and PP9984349 (held by D.B.). Animals were housed in specific pathogen-free conditions. Both male and female mice typically aged 6-8 weeks were used, and littermates of the same sex were randomly assigned to experimental groups.

Accelerated adaptive tolerance models and immunotherapy

Tg4 Nur77-Tempo *Il10*-GFP or Tg4 *Nr4a3*-Tocky *Il10*-GFP mice were immunized through subcutaneous injection of 4 mg/kg [4Y] MBP peptide PBS into the flank. For *in vivo* blockade experiments, antibodies were administrated via the intraperitoneal (i.p.) route with 0.5 mg of anti-PD-L1 antibody (clone MIH5(82)) or rat IgG2a (clone MAC219, kind gift from Professor Anne Cooke, University of Cambridge), *in vivo* grade anti-Lag3 (clone C9B7W BioLegend) or rat IgG1 (clone MAC221). For combination therapy experiments, anti-PD-L1 and anti-Lag3 or their corresponding isotype were pooled at 1:1 ratios. For re-challenge experiments, 30

minutes after immunotherapy administration a second dose of 0.4 mg/kg [4Y]-MBP peptide in PBS was administered subcutaneously to the contralateral flank. Mice were then euthanised at the indicated time points, and spleens removed to analyse systemic T cell responses.

Spleen processing and flow cytometry

Splenocytes were dissociated using scissors in 1.2 mL of digestion media containing 1 mg/mL collagenase D (Merck Life Sciences) and 0.1 mg/mL DNase I (Merck Life Sciences) in 1 % FBS (v/v) RPMI for 25 min at 37 °C in a thermo-shaker. Digested tissue was passed through a 70 µM filter (Greiner) and centrifuged at 1500 rpm for 5 min. Red blood cells were lysed in RBC lysis buffer (Invitrogen) for 2 mins on ice before washing in 2% FBS RPMI. Resulting sample was resuspended in FACS buffer (PBS, 2% FBS). Analysis was performed on a BD LSR Fortessa X-20 instrument. The blue form of the Timer protein was detected in the blue (450/40 nm) channel excited off the 405 nm laser. The red form of the Timer protein was detected in the mCherry (610/20 nm) channel excited off the 561 nm laser. A fixable eFluor780-flurescent viability dye (eBioscience) was used for all experiments. Directly conjugated antibodies used in these experiments were CD4 APC or PerCP-Cy5.5 (clone GK1.5, BioLegend), CD4, CD4 Alexa Fluor 700 (clone RM4-4, BioLegend), CD4 BUV737 (clone GK1.5, BD Biosciences),TCR Vβ8.1, 8.2 BUV395 (clone, MR5-2, BD Biosciences) CD4 BUV395 (clone GK1.5, BD Biosciences), CD8a PE-Cy7 (clone 53-6.7, BioLegend), TCRβ FITC (clone H57-597, BioLegend), PD1 PE-Cy7 (clone 29F.1A12, BioLegend), Lag3 APC or PE-Cy7 (clone C9B7W, BioLegend), OX40 APC or PE-Cy7 (clone OX-86, BioLegend), GITR PE-Cy7 or PerCPCy5.5. (clone DTA-1, BioLegend), ICOS Alexa Fluor 700 (clone C398.4A,

BioLegend), IRF8 PE (clone V3GYWCH, Invitrogen), CD25 PE-Cy7 (clone PC61, BioLegend), CD44 PerCP-Cy5.5. (clone IM7, BioLegend), PD-L1 APC or PE-Cy7 (clone 10F.9G2, BioLegend), IRF4 PE-Cy7 (clone IRF4.3E4, BioLegend), CCR6 APC or PE (clone 29-2L17, BioLegend), CXCR5 APC (clone L138D7, BioLegend), CD19 PE-Cy7 (clone 6D5, BioLegend), CD11b PE-Cy7 (clone M1/70, BioLegend), PD-L1 BV711 (clone 10F.9G2, BioLegend). For intracellular staining of IRF8 or IRF4, the Foxp3 transcription factor staining buffer kit was used according to the manufacturers' instructions (eBioscience). For cell sorting for RNA-seq experiments, single cell suspensions from the spleens of immunised mice were generated and then multiplexed to sort in batches of four on a FACS ARIA FUSION cell sorter (BD Biosciences). Multiplex sorting was performed using the following CD4 antibodies for the four experimental conditions: Isotype (CD4 APC), anti-PD-L1 (CD4 BUV395), anti-Lag3 (BUV737) and combination therapy (CD4 PerCPcy5.5). A dump channel consisting of CD19 PE-Cy7, CD11b PE-CY7 and CD8-Cy7 was used and cells were sorted as live, $CD4^{+}CD19^{-}CD11b^{-}CD8^{-}Nr4a3Red^{+}Nr4a3Blue^{+}$ (i.e. "responder" $CD4^{+}$ T cells). For migration assays live, $CD4^{+}CD19^{-}CD11b^{-}CD8^{-}$ were sorted.

In vitro restimulation of antigen adapted T cells (hybrid model)

For the hybrid tolerance model Tg4 *Nr4a3*-Tocky Tiger (*Il10*-GFP) mice were immunized through subcutaneous injection of 4 mg/kg [4Y] MBP peptide. 24 h later mice were euthanised and spleens were removed and digested as described above. Digested cells were washed once and $5x10^{5}$ splenocytes cultured for 24 h in 96-well U-bottom plates (Corning) final volume of 200 µl RPMI 1640 containing 10% FCS and penicillin/streptomycin and 55 µM β-mercaptoethanol (Gibco) for the stated time periods in the presence of a range of [4Y]-MBP peptide concentrations. Blocking

antibodies (anti-PD-L1 clone MIH5, and anti-Lag3 clone C9B7W) were administered at 20 µg/mL.

RNA-seq library preparation and analysis

RNA was extracted from lysates using the PureLink RNA Micro Scale Kit (Invitrogen) according to the manufacturer's instructions. 5 ng of RNA was used for generation of sequencing libraries using the Quantseq 3' mRNA-seq Library Preparation kit (Lexogen). Briefly, library generation was commenced with oligodT priming containing the Illumina-specific Read 2 linker sequence. After first strand synthesis, RNA was degraded. Second strand synthesis was initiated by random priming and a DNA polymerase. Random primers contained the illumina-specific Read 1 linker sequence. Double stranded DNA was purified from the reaction using magnetic beads and libraries amplified (18 cycles) and sequences required for cluster generation and sample indexes were introduced. Libraries were normalized and pooled at a concentration of 4 nM for sequencing. Libraries were sequenced using the NextSeq 500 using a High 75 cycle flow cell. Cluster generation and sequencing was then performed and FASTQ files generated. FASTQ files were then processed by Lexogen as follows: Trimming was performed using Cutadapt version 1.18, followed by mapping using STAR version 2.6.1a to the GRCm38 genome. Reads counting as performed using FeatureCounts version 1.6.4. Uniquely mapped read counts conts in the .txt format were used for further analysis using DESeq2 in R version 4.0(83). A DESeq dataset was created from a matrix of raw read count data. Data were filtered to remove genes with fewer than 30 reads across all samples. Log2 fold change estimates were generated using the DESeq algorithm and

shrinkage using the ashr algorithm(84) to estimate log2 fold changes (lfc). A lfc threshold of 0.2 was set and genes with an adjusted p value<0.05 and an s value<0.005 were used to filter out genes with low expression or negligible gene expression changes. Normalized read counts were transformed using the regularised log (rlog) transformation. Heatmap analysis was performed on the rlog transformed data using the R package gplots. For KEGG pathway analysis clusterProfiler(85), DOSE(86) and biomaRt(87) packages were used. Venn diagrams were generated using the CRAN package VennDiagram.

Analysis of published ChIP-Seq data

Data was analysed as previously described(31). Briefly, processed bigwig data files deposited in GEO: GSE64409 (were downloaded and hosted in CyVerse Discovery Environment (https://de.cyverse.org/de) and then mapped against the mm9 genome using the UCSC genome browser.

Analysis of Riaz and Gide cohorts

FPKM for *CCR6* or *CCL20* were extracted for melanoma patients from supplementary files appended to GEO: GSE 91061 (36), or generated as described previously(2). FPKM were converted to TPM(88) through dividing each gene level FPKM by the sum of all FPKM in annotated genes within that sample. This figure was then multiplied by $1^{e}6$ then offset by 0.01 to avoid 0 values. Patient responses were characterised as: complete remission (CR), partial remission (PR), stable disease (SD) or progressive disease (PD) as per Riaz et al. (36) and Gide et al. (37). For combined survival analysis, patients within each cohort were classified as High

or low based on their own cohorts median *CCR6* TPM expression and then pooled for Kaplan-Meier visualisation.

TCR signal duration termination by PP2 administration

Nr4a3-Tocky Tg4 Tiger mice were subcutaneously injected with 4 mg/kg [4Y] MBP peptide. Mice were culled 24 h later and spleens were dissociated and single cell suspensions of splenocytes were made using the digest method as described above. Cells were washed once and cultured at $5x10^5$ cells per well on 96-well U-bottom plates (Corning) in presence of 0.1 μM [4Y]-MBP peptide in a final volume of 200 μl RPMI1640 + L-glutamine (GIBCO) containing 10% FCS and 1% penicillin/streptomycin (Life Technologies). Inhibitors were dissolved in DMSO. PP2 (Sigma, 10 μM) was added at different time points. Cells were incubated at 37°C and 5% CO2 and analysed at the indicated time points on flow cytometry.

Immunization for Tfh cell responses

C57BL/6J mice were immunized with alum-precipitated (9% aluminum potassium sulfate (Sigma-Aldrich)) NP-OVA conjugate (NP-conjugated ovalbumin), alum NP-OVA. These were respectively prepared by mixing endotoxin-free NP-conjugated ova (kind gift from Prof Kai Toellner, University of Birmingham) with a 9% alum solution. Per mouse a total of 20 µg NP-OVA was mixed with same volume of 9% alum and pH was adjusted using NaOH and HCL. After washing, 20µg NP-ova/Alum was resuspended in a total volume of 20µl PBS and injected into the left footpad. 24 h later mice were administrated via the intraperitoneal (i.p.) route with 0.5 mg anti-PD-L1 (clone MIH5), anti-Lag3 (clone C9B7W), combination therapy of their respective isotype control (pooled at 1:1 ratios). On day 8, mice were euthanised and

the popliteal lymph node was harvested. LNs were forced through 70 µM filters, before cells were stained for flow cytometric analysis.

Analysis of human combination therapy datasets

Differentially expressed genes compared to month 3 or month 1 compared to baseline in CD4 Naïve, CD4 effector memory, and CD4 Treg clusters from human patients on anti-PD-1 and anti-Lag3 therapy were extracted from supplementary files from(38) and intersected with DEGs identified from Isotype and CB mice from Figure 3 (**Supplementary Table 1**).

Migration assays

To measure migration, FACS purified $CD4^+$ T cells were cultured in a 5 µm polycarbonate 24-well transwell system (Corning). T cells were loaded into the top chamber at a density of 2.5×10^5 cells in 0.1 mL complete media, with the bottom chamber containing either 0 or 100 ng/mL CCL20 (BioLegend) in 0.6 mL complete media. After 4 hours, the contents of the bottom chamber were harvested and washed extensively with PBS (+ 2 mM EDTA and 2% FCS), followed by enumeration by flow cytometry. AccuCheck couning beads (Invitrogen) were used to calculate the absolute number of $CD4^+$ T cells in each sample. Migration index was calculated by normalising cells in the lower chamber compared to the medium alone control from isotype-treated mice.

Statistical Analysis

For non-RNA-sequencing analysis, statistical analysis was performed on Prism 10 (GraphPad) software. Flow cytometry data were analyzed using FlowJo software

(BD Biosciences). Statistical analysis for comparison of more than two means was performed using One-Way ANOVA with Tukey's multiple comparisons test. For analysis of two factor variable experiments, a Two-way repeated measures ANOVA was performed with Tukey's multiple comparisons tests. For detection of synergy, a Two-way ANOVA test was performed factoring in the variables anti-PD-L1 and anti-Lag3 to test for significance of interaction. For non-parametric data a Kruskal Wallis test was performed with Dunn's multiple comparisons. For survival analysis, analysed a Log-rank (Mantel-Cox) test was used. For correlation analysis Spearman's rank was performed. Variance is reported as mean ± SEM unless stated otherwise; data points represent individual mice. $^{*}p = < 0.05$, $^{**}p = < 0.01$, $^{***}p = < 0.001$, $^{****}p = < 0.0001$.

Acknowledgements

Work is funded by an MRC Career Development award (MR/V009052/1 to D.B.) and a Lister Institute of Preventive Medicine Fellowship (to D.B.). We thank Genomics Birmingham for performing RNA-seq library preparation and sequencing. We thank the Birmingham Flow cytometry facility for support with cell sorting. Diagrams in the figures were generated using BioRender.com.

Figure Legends

Figure 1: PD-L1 pathway is dominant over Lag3 in controlling initial CD4$^+$ T cell activation

(**A**) Experimental setup and interpretation for part (**B**). (**B**) Tg4 Nur77-Tempo *Il10*-GFP mice were immunized s.c. with 4 mg/kg of [4Y]-MBP. 24 h later mice were randomized to receive either 0.5 mg isotype pool (1:1 ratio of rat IgG1 and rat IgG2a), anti-Lag3, or anti-PD-L1 or CT. 18 h after ICB mice were euthanized and splenic responses were analysed for Nur77-Timer Blue versus Nur77-Timer Red. (**B**) Flow cytometry plots showing expression of Nur77-Timer Blue versus Nur77-Timer Red cells at 18 h post ICB administration. (**C**) Summary data detailing the percentage of persistent TCR signalling CD4$^+$ T cells. (**D**) Summary data detailing median ICOS expression within persistently signalling CD4+ T cells (CD4$^+$Nur77-Timer Blue$^+$Nur77-Timer Red$^+$). Isotype (n = 9), anti-Lag3 (n = 10), or anti-PD1 (n =9) or CT (n=10); data pooled from two independent experiments. Bars represent mean ± SEM, dots represent individual mice. Statistical analysis by one-way ANOVA with Tukey's multiple comparisons test.

(**E**) Experimental setup and interpretation for part (**F-H**). (**F**) Mice were immunized with 20 µg NP-OVA/ alum in a total volume of 20 µl subcutaneously into the left foot pad. 24 h later mice were injected randomly either with 0.5 mg isotype pool (1:1 ratio of rat IgG1 and rat IgG2a), anti-Lag3, or anti-PD-L1 or combination treatment. At day 8 post immunization mice were sacrificed and popliteal lymph nodes were harvested for analysis by flow cytometry. Flow cytometry plots showing expression of PD-1 versus CXCR5 or CD4 versus ICOS in live CD4$^+$ T cells. (**G-H**) summary data detailing the percentage of Tfh cells **(G**), ICOS median in CD4$^+$ T cells (**H**) or ICOS median in Tfh cells (**E**). Isotype (n=14), anti-Lag3 (n = 14), anti-PD1 (n =14) or

combination therapy (n=13), data are pooled from two independent experiments. Bars represent mean ± SEM (**C, D** and **H**) or median (**G**), dots represent individual mice. Statistical analysis by one-way ANOVA with Tukey's multiple comparisons test (**C, D**, **H**) or Kruskal Wallis test with Dunn's multiple comparisons test (**G**).

Figure 2: Lag3 and PD-L1 pathways exert additive and synergistic effects on CD4$^+$ T cell activation during secondary stimulation

(**A**) Experimental setup and interpretation for part (B). (**B**) Tg4 *Nr4a3*-Tocky *Il10*-GFP mice were immunized s.c. with 4 mg/kg of [4Y] MBP. 24 h later mice were randomized to receive either 0.5 mg isotype pool (1:1 ratio of rat IgG1 and rat IgG2a), anti-Lag3, or anti-PD-L1 or a combination of both 30 min prior to re-challenge with 0.4 mg/kg [4Y] MBP peptide. Splenic CD4$^+$ T cells were analyzed for *Nr4a3*-Blue versus *Nr4a3*-Red analysis at 12 h after peptide re-challenge. Flow plots showing expression of OX40 and ICOS within CD4$^+$ T cells. (**C**) Summary data from (B) detailing percentage of responders after 12 h re-challenge. (**D**) and Summary data from (B) detailing MFI (median fluorescence intensity) of OX40 and ICOS within responding CD4$^+$ T cells after 12 h re-challenge. (**E**) Summary data detailing geometric mean of ICOS and OX40 (surface TCR.strong) after 12 h re-challenge. (**C**)-(**E**) Isotype (n = 7), anti-Lag3 (n = 7), or anti-PD1 (n =8) or combination therapy (n=8). Bars represent mean ± SEM, dots represent individual mice. Statistical analysis by one-way ANOVA with Tukey's multiple comparisons test. Two-way anova to test the interaction effects of percentage responders and geometric mean of surface TCR.strong between αLag3 and αPD-L1 at (**F**) 12 h (IgG

n=7, anti-PD-L1=7, anti-Lag3=8, and combination n=8) or 18 h (**G**) post re-challenge (IgG n=8, anti-PD-L1=8, anti-Lag3=10, and combination n=10).

Figure 3: Transcriptional analysis reveals Th17/Tfh cell bias and activation of an NFAT-biased gene signature in response to Lag3 and PD-L1 blockade

(**A**) Experimental setup and interpretation for part (B). (**B**) Tg4 *Nr4a3*-Tocky *Il10*-GFP mice were immunized s.c. with 4 mg/kg of [4Y]-MBP. 24 h later mice were randomized to receive either 0.5 mg isotype pool (n=3) (1:1 ratio of rat IgG1 and rat IgG2a), anti-Lag3 (n=3), or anti-PD-L1 (n=3) or combination therapy (n=3) 30 min prior to re-challenge with 0.4 mg/kg [4Y]-MBP peptide. 12 h later splenic $CD4^+$ T cell responses were analyzed for *Nr4a3*-Timer Red versus *Nr4a3*-Timer Blue expression in live $CD4^+$ Tg4 T cells and sorted for $CD4^+$Nr4a3-$Blue^+$Nr4a3-Red+ T cells by FACS. (**B**) Flow plots showing *Nr4a3*-Timer $Blue^+$, *Nr4a3*-Timer Red^+ pre and post sorting. (**C**) RNA was extracted from the sorted populations and 3′ mRNA sequencing performed. PCA of the normalized expression data identifies 4 clusters. Venn diagram analysis of up (**D**) or down (**E**) regulated DEGs in mice receiving combination therapy compared to the three other experimental conditions. (**F**) Z score heatmap analysis of rLog expression of genes involved in $CD4^+$ T helper subsets from Isotype (IgG), anti-Lag3, anti-PD-L1 or CB treated mice. (**G**) Intersection of the 189 genes that were upregulated in $CD4^+$ T cell responders between CB treated and Isotype-treated mice with the 1089 identified in Wither et al.(32) (**H**) Heatmap visualisation of the 39 genes overlapping from (**G**) across the treatment groups. Annotation of dependency of NFAT/ERK signalling is based on classification from Wither et al(32).

Figure 4: Combination blockade biases towards Tfh cell development and synergistically upregulates CCR6

(**A**) Experimental setup and interpretation for part (**B**). Tg4 Nur77-Tempo *Il10*-GFP mice were immunized s.c. with 4 mg/kg of [4Y]-MBP. 24 h later mice were randomized to receive either 0.5 mg isotype pool (1:1 ratio of rat IgG1 and rat IgG2a), anti-Lag3, or anti-PD-L1 or CT 30 min prior to re-challenge with 0.4 mg/kg [4Y]-MBP peptide. 18 h later mice were euthanised and splenic responses were analysed for PD-1, CXCR5 and ICOS expression. (**C**) Frequency of Tfh cells amongst the $CD4^+$ T cells, (**D**) median ICOS expression in $CD4^+$ T cells or median ICOS expression in Tfh cells (**E**). Isotype (n=4), anti-Lag3 (n =5), anti-PD1 (n =5) or CT (n=5). (**F-I**) Tg4 *Nr4a3*-Tocky *Il10*-GFP mice were immunized s.c. with 4 mg/kg of [4Y]-MBP. 24 h later mice were randomized to receive either 0.5 mg isotype pool (1:1 ratio of rat IgG1 and rat IgG2a), anti-Lag3, or anti-PD-L1 or a combination therapy 30 min prior to re-challenge with 0.4 mg/kg [4Y]-MBP peptide. 12 h later mice were euthanised and splenic responses were analysed by flow cytometry. (**F**) Flow cytometry plots showing expression of IRF8 and IRF4 in total $CD4^+$ T cells and (**G**) summary data showing median expression levels of IRF8 and IRF4. (**H**) Flow cytometry plots showing CCR6 expression (gated on responder T cells) and (**I**) Two-way anova to test the interaction for the treatments in driving expression of CCR6. (**F**)-(**I**) Isotype (n=5), anti-Lag3 (n=5), or anti-PD1 (n=5) or CB treatment (n=6). Bars represent mean ± SEM, dots represent individual mice. Statistical analysis by one-way ANOVA with Tukey's multiple comparisons test. (**J**). Statistical analysis by repeated measures two-way ANOVA with Tukey's multiple comparisons test.

Figure 5: PD-L1 and Lag3 co-operatively regulate TCR signal duration in CD4$^+$ T cells

(**A**) Graphical illustration of the levels of Nr4a3-Blue and Nr4a3-Red following a short or prolonged TCR signal. Tg4 *Nr4a3*-Tocky *Il10*-GFP mice were immunized s.c. with 4 mg/kg of [4Y]-MBP. 24 h later mice were randomized to receive either 0.5 mg isotype pool (1:1 ratio of rat IgG1 and rat IgG2a), anti-Lag3, or anti-PD-L1 or CT 30 min prior to re-challenge with 0.4 mg/kg [4Y] MBP peptide. 12 h and 18 h later mice were culled and splenic responses were analysed for *Nr4a3*-Timer Red expression in responder populations. (**B**) Summary of data at 12 h post re-challenge showing red median within responders. Isotype (n = 7), anti-Lag3 (n = 7), or anti-PD1 (n =8) or combination (n=8). Bars represent mean ± SEM, dots represent individual mice. Statistical analysis by one-way ANOVA with Tukey's multiple comparisons test. (**C**) Summary of data at 18 h post re-challenge showing Timer Red median within responders. Isotype (n =4), anti-Lag3 (n = 5), or anti-PD1 (n =5) or combination (n=5). Bars represent mean ± SEM, dots represent individual mice. (**D**) Experimental setup and interpretation for part (E). Mice were immunized s.c. with 4 mg/kg of [4Y]-MBP (n=6). 24 h later mice were euthanised, and spleens were harvested. Splenocytes were cultured with 0.1 μM [4Y]-MBP for another 24 h and 10 μM PP2 was added to terminate TCR signalling at different time points (0 h, 4 h, 8 h and 12 h and 24 h) before analysis by flow cytometry. (**E**) Summary data showing MFI (median fluorescence intensity) of *Nr4a3*-Timer Blue, ICOS, OX40 or IRF8 in response to different duration of TCR signalling. Statistical analysis by one-way ANOVA with Tukey's multiple comparisons test.

Figure 6: Elevated Tumour *CCR6* expression associates with enhanced survival in melanoma patients on PD-1 pathway targeting immunotherapies

CCR6 TPM in pre-therapy (**A,** CR/PR n=10, SD, n=16, PD n=23) or on-therapy (**B,** CR/PR n=13, SD, n=18, PD n=24) tumour biopsy from Riaz et al.(36) cohort. (CR=complete response, PR=partial response, SD=stable disease, PD=progressive disease). Patients were assigned to high (black line) or low (red line) groups based on their on-therapy tumour *CCR6* expression compared to the whole cohort median. Patients were then split according to whether they were ipilimumab naïve (**C,** High n=11, Low, n=10) or ipilimumab progressed (**D,** High n=14, Low n=15) onto Nivolumab treatment Kaplan-Meier curves generated for analysis of overall survival. (**E**) correlation of *CCR6* versus *CCL20* TPM within all on-treatment biopsies from Riaz et al.(36) (including those without RECIST classification) by Spearman's Rank analysis (n=57). (**F**) Analysis of early during treatment tumour biopsy of melanoma patients on PD-1/PD-L1 incorporating immunotherapy from the Gide et al.(37) study (CR/PR n=9, SD n=2, PD n=7). (**G**) Combined overall survival analysis of patients from the Riaz et al.(36) and Gide et al.(37) cohorts stratified by high (n=34) or low (n=34) on-treatment tumour *CCR6* expression levels. Bars represent median and interquartile range (A,B,F).

Figure 7: CCR6 upregulation in human effector memory CD4$^+$ T cells on Nivolumab and Relatlimab combination therapy

(**A**) Differentially expressed genes compared to month 3 or month 1 compared to baseline in CD4 Naïve or central memory, CD4 effector memory, and CD4 Treg clusters from human patients on anti-PD-1 and anti-Lag3 therapy were extracted from supplementary files from Huuhtanen *et al*. (38) and intersected with DEGs

identified from Isotype and combination treated mice from Figure 2 (Supplementary Table 1). (**B**) displays genes upregulated in subsets. (**C**) displays genes downregulated in the subsets. CM= central memory, EM=effector memory. (**D**) $CD4^+$ T cells were FACS purified and cultured in transwells with either 0 or 100 ng/mL of CCL20. 4 hours later the migration index was calculated for the four experimental conditions (Isotype (n=6), anti-Lag3 (n=8), or anti-PD1 (n=8) or CT (n=8), pooled from two independent experiments.

Supplementary Figures and Tables

Supplementary Figure 1: Gating strategy and generation of surface TCR.strong metric

Supplementary Figure 2: NFAT binding of key genes identified in Figure 3

University of California, Santa Cruz (UCSC) genome browser tracks showing NFAT1 binding peaks in $P14^+$ *Tcra*$^{-/-}$ $CD8^+$ T cells from GEO: GSE64409 at the genes *Nr4a3*, *Icos*, *Irf8* and *Tnfrsf4*.

Supplementary Figure 3: Combination therapy can modulate TCR signal strength in antigen adapted T cells in vitro

(A) Tg4 *Nr4a3*-Tocky *Il10*-GFP mice were immunized s.c. with 4 mg/kg of [4Y]-MBP peptide. 24 h post immunisation splenocytes were cultured for another 24 h and rechallenged with 0, 2.5, 10, 40 nM [4Y]-MBP peptide in presence of isotype pool, α-PD-L1, αLag-3, or a combination of PD-L1 and αLag-3. Splenic $CD4^+$ T cell responses were analyzed for OX40 and ICOS within the responding T cells after 24 h culture. (**B**) Summary data from (**A**) detailing MFI (median fluorescence intensity)

of OX40 and ICOS within responding $CD4^+$ T cells after 24 h culture. Bars represent mean ± SEM. Statistical analysis by two-way repeated measures ANOVA with Tukey's multiple comparisons test.

Supplementary Table 1: DEGs between Isotype, anti-PD-L1 and anti-Lag3 and CB treated groups

Supplementary Table 2: *CCR6* and *CCL20* TPM in Riaz Cohort and clinical data for on therapy samples

Supplementary Table 3: *CCR6* TPM in Gide Cohort and clinical data for early during treatment samples

References

1. Smith-Garvin JE, Koretzky GA, and Jordan MS. T cell activation. *Annu Rev Immunol.* 2009;27:591-619.
2. Elliot TAE, Jennings EK, Lecky DAJ, Thawait N, Flores-Langarica A, Copland A, et al. Antigen and checkpoint receptor engagement recalibrates T cell receptor signal strength. *Immunity.* 2021;54(11):2481-96 e6.
3. Nishimura H, Nose M, Hiai H, Minato N, and Honjo T. Development of lupus-like autoimmune diseases by disruption of the PD-1 gene encoding an ITIM motif-carrying immunoreceptor. *Immunity.* 1999;11(2):141-51.
4. Krummel MF, and Allison JP. CD28 and CTLA-4 have opposing effects on the response of T cells to stimulation. *J Exp Med.* 1995;182(2):459-65.
5. Workman CJ, and Vignali DA. The CD4-related molecule, LAG-3 (CD223), regulates the expansion of activated T cells. *Eur J Immunol.* 2003;33(4):970-9.
6. Freeman GJ, Long AJ, Iwai Y, Bourque K, Chernova T, Nishimura H, et al. Engagement of the PD-1 immunoinhibitory receptor by a novel B7 family member leads to negative regulation of lymphocyte activation. *J Exp Med.* 2000;192(7):1027-34.
7. Wolchok JD, Rollin L, and Larkin J. Nivolumab and Ipilimumab in Advanced Melanoma. *N Engl J Med.* 2017;377(25):2503-4.
8. Tawbi HA, Schadendorf D, Lipson EJ, Ascierto PA, Matamala L, Castillo Gutierrez E, et al. Relatlimab and Nivolumab versus Nivolumab in Untreated Advanced Melanoma. *N Engl J Med.* 2022;386(1):24-34.
9. Okazaki T, Maeda A, Nishimura H, Kurosaki T, and Honjo T. PD-1 immunoreceptor inhibits B cell receptor-mediated signaling by recruiting src homology 2-domain-containing tyrosine phosphatase 2 to phosphotyrosine. *Proc Natl Acad Sci U S A.* 2001;98(24):13866-71.
10. Mizuno R, Sugiura D, Shimizu K, Maruhashi T, Watada M, Okazaki IM, et al. PD-1 Primarily Targets TCR Signal in the Inhibition of Functional T Cell Activation. *Front Immunol.* 2019;10:630.
11. Hui E, Cheung J, Zhu J, Su X, Taylor MJ, Wallweber HA, et al. T cell costimulatory receptor CD28 is a primary target for PD-1-mediated inhibition. *Science.* 2017;355(6332):1428-33.
12. Linsley PS, Brady W, Urnes M, Grosmaire LS, Damle NK, and Ledbetter JA. CTLA-4 is a second receptor for the B cell activation antigen B7. *J Exp Med.* 1991;174(3):561-9.
13. Freeman GJ, Borriello F, Hodes RJ, Reiser H, Gribben JG, Ng JW, et al. Murine B7-2, an alternative CTLA4 counter-receptor that costimulates T cell proliferation and interleukin 2 production. *J Exp Med.* 1993;178(6):2185-92.
14. Freeman GJ, Gribben JG, Boussiotis VA, Ng JW, Restivo VA, Jr., Lombard LA, et al. Cloning of B7-2: a CTLA-4 counter-receptor that costimulates human T cell proliferation. *Science.* 1993;262(5135):909-11.
15. Walker LS, and Sansom DM. Confusing signals: recent progress in CTLA-4 biology. *Trends Immunol.* 2015;36(2):63-70.
16. Triebel F, Jitsukawa S, Baixeras E, Roman-Roman S, Genevee C, Viegas-Pequignot E, et al. LAG-3, a novel lymphocyte activation gene closely related to CD4. *J Exp Med.* 1990;171(5):1393-405.

17. Baixeras E, Huard B, Miossec C, Jitsukawa S, Martin M, Hercend T, et al. Characterization of the lymphocyte activation gene 3-encoded protein. A new ligand for human leukocyte antigen class II antigens. *J Exp Med.* 1992;176(2):327-37.
18. Bawden EG, Wagner T, Schroder J, Effern M, Hinze D, Newland L, et al. CD4(+) T cell immunity against cutaneous melanoma encompasses multifaceted MHC II-dependent responses. *Sci Immunol.* 2024;9(91):eadi9517.
19. Bos R, and Sherman LA. CD4+ T-cell help in the tumor milieu is required for recruitment and cytolytic function of CD8+ T lymphocytes. *Cancer Res.* 2010;70(21):8368-77.
20. Zhu Z, Cuss SM, Singh V, Gurusamy D, Shoe JL, Leighty R, et al. CD4+ T Cell Help Selectively Enhances High-Avidity Tumor Antigen-Specific CD8+ T Cells. *J Immunol.* 2015;195(7):3482-9.
21. Vafaei S, Zekiy AO, Khanamir RA, Zaman BA, Ghayourvahdat A, Azimizonuzi H, et al. Combination therapy with immune checkpoint inhibitors (ICIs); a new frontier. *Cancer Cell Int.* 2022;22(1):2.
22. Long GV, Hodi FS, Lipson EJ, Schadendorf D, Ascierto PA, Matamala L, et al. Overall Survival and Response with Nivolumab and Relatlimab in Advanced Melanoma. *NEJM Evidence.* 2023;2(4):EVIDoa2200239.
23. Hodi FS, Chiarion-Sileni V, Gonzalez R, Grob JJ, Rutkowski P, Cowey CL, et al. Nivolumab plus ipilimumab or nivolumab alone versus ipilimumab alone in advanced melanoma (CheckMate 067): 4-year outcomes of a multicentre, randomised, phase 3 trial. *Lancet Oncol.* 2018;19(11):1480-92.
24. Correa K, and Dustin ML. Locked and loaded: strong TCR signaling primes anti-PD-1 therapy. *Trends Immunol.* 2021;42(12):1066-8.
25. Anderton SM, Manickasingham SP, Burkhart C, Luckcuck TA, Holland SJ, Lamont AG, et al. Fine specificity of the myelin-reactive T cell repertoire: implications for TCR antagonism in autoimmunity. *J Immunol.* 1998;161(7):3357-64.
26. Fairchild PJ, Wildgoose R, Atherton E, Webb S, and Wraith DC. An autoantigenic T cell epitope forms unstable complexes with class II MHC: a novel route for escape from tolerance induction. *Int Immunol.* 1993;5(9):1151-8.
27. Fugger L, Liang J, Gautam A, Rothbard JB, and McDevitt HO. Quantitative analysis of peptides from myelin basic protein binding to the MHC class II protein, I-Au, which confers susceptibility to experimental allergic encephalomyelitis. *Mol Med.* 1996;2(2):181-8.
28. Maruhashi T, Okazaki IM, Sugiura D, Takahashi S, Maeda TK, Shimizu K, et al. LAG-3 inhibits the activation of CD4(+) T cells that recognize stable pMHCII through its conformation-dependent recognition of pMHCII. *Nat Immunol.* 2018;19(12):1415-26.
29. Maruhashi T, Sugiura D, Okazaki IM, Shimizu K, Maeda TK, Ikubo J, et al. Binding of LAG-3 to stable peptide-MHC class II limits T cell function and suppresses autoimmunity and anti-cancer immunity. *Immunity.* 2022;55(5):912-24 e8.
30. Subach FV, Subach OM, Gundorov IS, Morozova KS, Piatkevich KD, Cuervo AM, et al. Monomeric fluorescent timers that change color from blue to red report on cellular trafficking. *Nat Chem Biol.* 2009;5(2):118-26.

31. Jennings E, Elliot TAE, Thawait N, Kanabar S, Yam-Puc JC, Ono M, et al. Nr4a1 and Nr4a3 Reporter Mice Are Differentially Sensitive to T Cell Receptor Signal Strength and Duration. *Cell Rep.* 2020;33(5):108328.
32. Wither MJ, White WL, Pendyala S, Leanza PJ, Fowler DM, and Kueh HY. Antigen perception in T cells by long-term Erk and NFAT signaling dynamics. *Proc Natl Acad Sci U S A.* 2023;120(52):e2308366120.
33. Martinez GJ, Pereira RM, Aijo T, Kim EY, Marangoni F, Pipkin ME, et al. The transcription factor NFAT promotes exhaustion of activated CD8(+) T cells. *Immunity.* 2015;42(2):265-78.
34. Merkenschlager J, Finkin S, Ramos V, Kraft J, Cipolla M, Nowosad CR, et al. Dynamic regulation of TFH selection during the germinal centre reaction. *Nature.* 2021;591(7850):458-63.
35. Seth A, Yokokura Y, Choi JY, Shyer JA, Vidyarthi A, and Craft J. AP-1-independent NFAT signaling maintains follicular T cell function in infection and autoimmunity. *J Exp Med.* 2023;220(5).
36. Riaz N, Havel JJ, Makarov V, Desrichard A, Urba WJ, Sims JS, et al. Tumor and Microenvironment Evolution during Immunotherapy with Nivolumab. *Cell.* 2017;171(4):934-49 e16.
37. Gide TN, Quek C, Menzies AM, Tasker AT, Shang P, Holst J, et al. Distinct Immune Cell Populations Define Response to Anti-PD-1 Monotherapy and Anti-PD-1/Anti-CTLA-4 Combined Therapy. *Cancer Cell.* 2019;35(2):238-55 e6.
38. Huuhtanen J, Kasanen H, Peltola K, Lonnberg T, Glumoff V, Bruck O, et al. Single-cell characterization of anti-LAG-3 and anti-PD-1 combination treatment in patients with melanoma. *J Clin Invest.* 2023;133(6).
39. Reissig S, Tang Y, Nikolaev A, Gerlach K, Wolf C, Davari K, et al. Elevated levels of Bcl-3 inhibits Treg development and function resulting in spontaneous colitis. *Nat Commun.* 2017;8:15069.
40. Yu X, Teng XL, Wang F, Zheng Y, Qu G, Zhou Y, et al. Metabolic control of regulatory T cell stability and function by TRAF3IP3 at the lysosome. *J Exp Med.* 2018;215(9):2463-76.
41. Cornely R, Pollock AH, Rentero C, Norris SE, Alvarez-Guaita A, Grewal T, et al. Annexin A6 regulates interleukin-2-mediated T-cell proliferation. *Immunol Cell Biol.* 2016;94(6):543-53.
42. Yu H, Leitenberg D, Li B, and Flavell RA. Deficiency of small GTPase Rac2 affects T cell activation. *J Exp Med.* 2001;194(7):915-26.
43. Glatigny S, Duhen R, Oukka M, and Bettelli E. Cutting edge: loss of alpha4 integrin expression differentially affects the homing of Th1 and Th17 cells. *J Immunol.* 2011;187(12):6176-9.
44. Boussiotis VA. Molecular and Biochemical Aspects of the PD-1 Checkpoint Pathway. *N Engl J Med.* 2016;375(18):1767-78.
45. Kouo T, Huang L, Pucsek AB, Cao M, Solt S, Armstrong T, et al. Galectin-3 Shapes Antitumor Immune Responses by Suppressing CD8+ T Cells via LAG-3 and Inhibiting Expansion of Plasmacytoid Dendritic Cells. *Cancer Immunol Res.* 2015;3(4):412-23.
46. Wang J, Sanmamed MF, Datar I, Su TT, Ji L, Sun J, et al. Fibrinogen-like Protein 1 Is a Major Immune Inhibitory Ligand of LAG-3. *Cell.* 2019;176(1-2):334-47 e12.

47. Guy C, Mitrea DM, Chou PC, Temirov J, Vignali KM, Liu X, et al. LAG3 associates with TCR-CD3 complexes and suppresses signaling by driving co-receptor-Lck dissociation. *Nat Immunol.* 2022;23(5):757-67.
48. Aggarwal V, Workman CJ, and Vignali DAA. LAG-3 as the third checkpoint inhibitor. *Nat Immunol.* 2023;24(9):1415-22.
49. Li N, Wang Y, Forbes K, Vignali KM, Heale BS, Saftig P, et al. Metalloproteases regulate T-cell proliferation and effector function via LAG-3. *EMBO J.* 2007;26(2):494-504.
50. Andrews LP, Somasundaram A, Moskovitz JM, Szymczak-Workman AL, Liu C, Cillo AR, et al. Resistance to PD1 blockade in the absence of metalloprotease-mediated LAG3 shedding. *Sci Immunol.* 2020;5(49).
51. Fife BT, Pauken KE, Eagar TN, Obu T, Wu J, Tang Q, et al. Interactions between PD-1 and PD-L1 promote tolerance by blocking the TCR-induced stop signal. *Nat Immunol.* 2009;10(11):1185-92.
52. Schneider H, Downey J, Smith A, Zinselmeyer BH, Rush C, Brewer JM, et al. Reversal of the TCR stop signal by CTLA-4. *Science.* 2006;313(5795):1972-5.
53. Woo SR, Turnis ME, Goldberg MV, Bankoti J, Selby M, Nirschl CJ, et al. Immune inhibitory molecules LAG-3 and PD-1 synergistically regulate T-cell function to promote tumoral immune escape. *Cancer Res.* 2012;72(4):917-27.
54. Speiser DE, Chijioke O, Schaeuble K, and Munz C. CD4(+) T cells in cancer. *Nat Cancer.* 2023;4(3):317-29.
55. Kos K, and de Visser KE. The Multifaceted Role of Regulatory T Cells in Breast Cancer. *Annu Rev Cancer Biol.* 2021;5:291-310.
56. Satpathy AT, Granja JM, Yost KE, Qi Y, Meschi F, McDermott GP, et al. Massively parallel single-cell chromatin landscapes of human immune cell development and intratumoral T cell exhaustion. *Nat Biotechnol.* 2019;37(8):925-36.
57. Gutierrez-Melo N, and Baumjohann D. T follicular helper cells in cancer. *Trends Cancer.* 2023;9(4):309-25.
58. Gu-Trantien C, Loi S, Garaud S, Equeter C, Libin M, de Wind A, et al. CD4(+) follicular helper T cell infiltration predicts breast cancer survival. *J Clin Invest.* 2013;123(7):2873-92.
59. Cui C, Wang J, Fagerberg E, Chen PM, Connolly KA, Damo M, et al. Neoantigen-driven B cell and CD4 T follicular helper cell collaboration promotes anti-tumor CD8 T cell responses. *Cell.* 2021;184(25):6101-18 e13.
60. Herati RS, Knorr DA, Vella LA, Silva LV, Chilukuri L, Apostolidis SA, et al. PD-1 directed immunotherapy alters Tfh and humoral immune responses to seasonal influenza vaccine. *Nat Immunol.* 2022;23(8):1183-92.
61. Jing Y, Liu J, Ye Y, Pan L, Deng H, Wang Y, et al. Multi-omics prediction of immune-related adverse events during checkpoint immunotherapy. *Nat Commun.* 2020;11(1):4946.
62. Tsukamoto H, Komohara Y, Tomita Y, Miura Y, Motoshima T, Imamura K, et al. Aging-associated and CD4 T-cell-dependent ectopic CXCL13 activation predisposes to anti-PD-1 therapy-induced adverse events. *Proc Natl Acad Sci U S A.* 2022;119(29):e2205378119.
63. Tafuri A, Shahinian A, Bladt F, Yoshinaga SK, Jordana M, Wakeham A, et al. ICOS is essential for effective T-helper-cell responses. *Nature.* 2001;409(6816):105-9.

64. Festen EA, Goyette P, Scott R, Annese V, Zhernakova A, Lian J, et al. Genetic variants in the region harbouring IL2/IL21 associated with ulcerative colitis. *Gut.* 2009;58(6):799-804.
65. Wellcome Trust Case Control C. Genome-wide association study of 14,000 cases of seven common diseases and 3,000 shared controls. *Nature.* 2007;447(7145):661-78.
66. Chat V, Ferguson R, Simpson D, Kazlow E, Lax R, Moran U, et al. Autoimmune genetic risk variants as germline biomarkers of response to melanoma immune-checkpoint inhibition. *Cancer Immunol Immunother.* 2019;68(6):897-905.
67. Rivino L, Gruarin P, Haringer B, Steinfelder S, Lozza L, Steckel B, et al. CCR6 is expressed on an IL-10-producing, autoreactive memory T cell population with context-dependent regulatory function. *J Exp Med.* 2010;207(3):565-77.
68. Kastirr I, Maglie S, Paroni M, Alfen JS, Nizzoli G, Sugliano E, et al. IL-21 is a central memory T cell-associated cytokine that inhibits the generation of pathogenic Th1/17 effector cells. *J Immunol.* 2014;193(7):3322-31.
69. Kadomoto S, Izumi K, and Mizokami A. The CCL20-CCR6 Axis in Cancer Progression. *Int J Mol Sci.* 2020;21(15).
70. Jin L, Cao L, Zhu Y, Cao J, Li X, Zhou J, et al. Enhance anti-lung tumor efficacy of chimeric antigen receptor-T cells by ectopic expression of C-C motif chemokine receptor 6. *Sci Bull (Beijing).* 2021;66(8):803-12.
71. Korn T, Bettelli E, Oukka M, and Kuchroo VK. IL-17 and Th17 Cells. *Annu Rev Immunol.* 2009;27:485-517.
72. Liao F, Rabin RL, Smith CS, Sharma G, Nutman TB, and Farber JM. CC-chemokine receptor 6 is expressed on diverse memory subsets of T cells and determines responsiveness to macrophage inflammatory protein 3 alpha. *J Immunol.* 1999;162(1):186-94.
73. Schmitt N, Bentebibel SE, and Ueno H. Phenotype and functions of memory Tfh cells in human blood. *Trends Immunol.* 2014;35(9):436-42.
74. Hirota K, Yoshitomi H, Hashimoto M, Maeda S, Teradaira S, Sugimoto N, et al. Preferential recruitment of CCR6-expressing Th17 cells to inflamed joints via CCL20 in rheumatoid arthritis and its animal model. *J Exp Med.* 2007;204(12):2803-12.
75. Yamazaki T, Yang XO, Chung Y, Fukunaga A, Nurieva R, Pappu B, et al. CCR6 regulates the migration of inflammatory and regulatory T cells. *J Immunol.* 2008;181(12):8391-401.
76. Lozano AX, Chaudhuri AA, Nene A, Bacchiocchi A, Earland N, Vesely MD, et al. T cell characteristics associated with toxicity to immune checkpoint blockade in patients with melanoma. *Nat Med.* 2022;28(2):353-62.
77. Aigner-Radakovics K, De Sousa Linhares A, Salzer B, Lehner M, Izadi S, Castilho A, et al. The ligand-dependent suppression of TCR signaling by the immune checkpoint receptor LAG3 depends on the cytoplasmic RRFSALE motif. *Sci Signal.* 2023;16(805):eadg2610.
78. Fernandes RA, Su L, Nishiga Y, Ren J, Bhuiyan AM, Cheng N, et al. Immune receptor inhibition through enforced phosphatase recruitment. *Nature.* 2020;586(7831):779-84.
79. Bending D, Prieto Martin P, Paduraru A, Ducker C, Marzaganov E, Laviron M, et al. A timer for analyzing temporally dynamic changes in transcription during differentiation in vivo. *J Cell Biol.* 2018;217(8):2931-50.

80. Burton BR, Britton GJ, Fang H, Verhagen J, Smithers B, Sabatos-Peyton CA, et al. Sequential transcriptional changes dictate safe and effective antigen-specific immunotherapy. *Nat Commun.* 2014;5:4741.
81. Elliot TAE, Jennings EK, Lecky DAJ, Rouvray S, Mackie GM, Scarfe L, et al. Nur77-Tempo mice reveal T cell steady state antigen recognition. *Discov Immunol.* 2022;1(1):kyac009.
82. Tsushima F, Iwai H, Otsuki N, Abe M, Hirose S, Yamazaki T, et al. Preferential contribution of B7-H1 to programmed death-1-mediated regulation of hapten-specific allergic inflammatory responses. *Eur J Immunol.* 2003;33(10):2773-82.
83. Love MI, Huber W, and Anders S. Moderated estimation of fold change and dispersion for RNA-seq data with DESeq2. *Genome Biol.* 2014;15(12):550.
84. Stephens M. False discovery rates: a new deal. *Biostatistics.* 2017;18(2):275-94.
85. Yu G, Wang LG, Han Y, and He QY. clusterProfiler: an R package for comparing biological themes among gene clusters. *OMICS.* 2012;16(5):284-7.
86. Yu G, Wang LG, Yan GR, and He QY. DOSE: an R/Bioconductor package for disease ontology semantic and enrichment analysis. *Bioinformatics.* 2015;31(4):608-9.
87. Durinck S, Spellman PT, Birney E, and Huber W. Mapping identifiers for the integration of genomic datasets with the R/Bioconductor package biomaRt. *Nat Protoc.* 2009;4(8):1184-91.
88. Pachter L. Models for transcript quantification from RNA-Seq. *arXiv.* 2011.

Figure 1

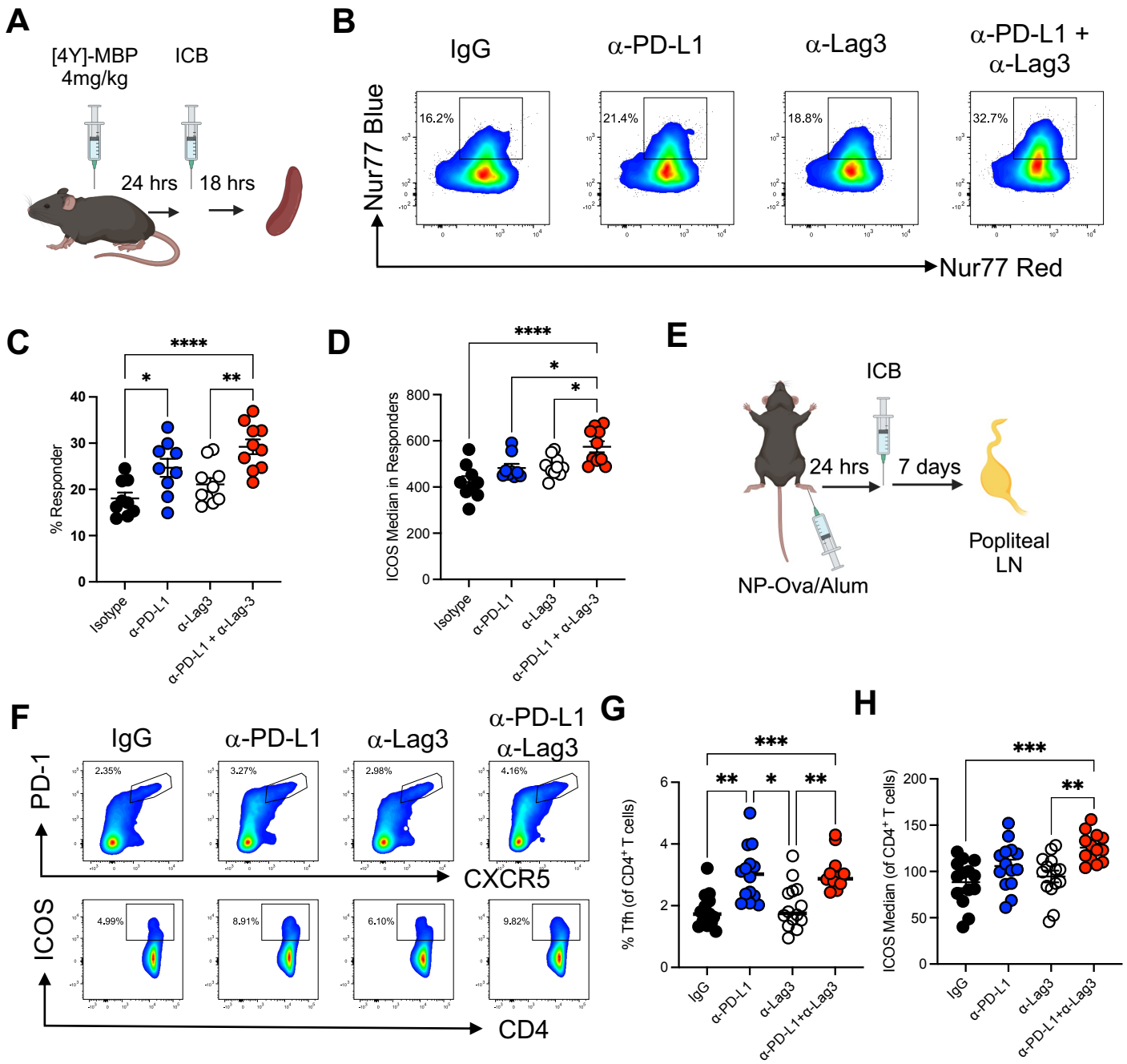
A
[4Y]-MBP
4mg/kg
ICB
24 hrs
18 hrs
B
IgG
α-PD-L1
α-Lag3
α-PD-L1 +
α-Lag3
Nur77 Blue
Nur77 Red
16.2%
21.4%
18.8%
32.7%
C
% Responder
Isotype
α-PD-L1
α-Lag3
α-PD-L1 + α-Lag-3
D
ICOS Median in Responders
E
ICB
24 hrs
7 days
NP-Ova/Alum
Popliteal
LN
F
IgG
α-PD-L1
α-Lag3
α-PD-L1
α-Lag3
PD-1
CXCR5
ICOS
CD4
2.35%
3.27%
2.98%
4.16%
4.99%
8.91%
6.10%
9.82%
G
% Tfh (of CD4+ T cells)
IgG
α-PD-L1
α-Lag3
α-PD-L1+α-Lag3
H
ICOS Median (of CD4+ T cells)

Figure 2

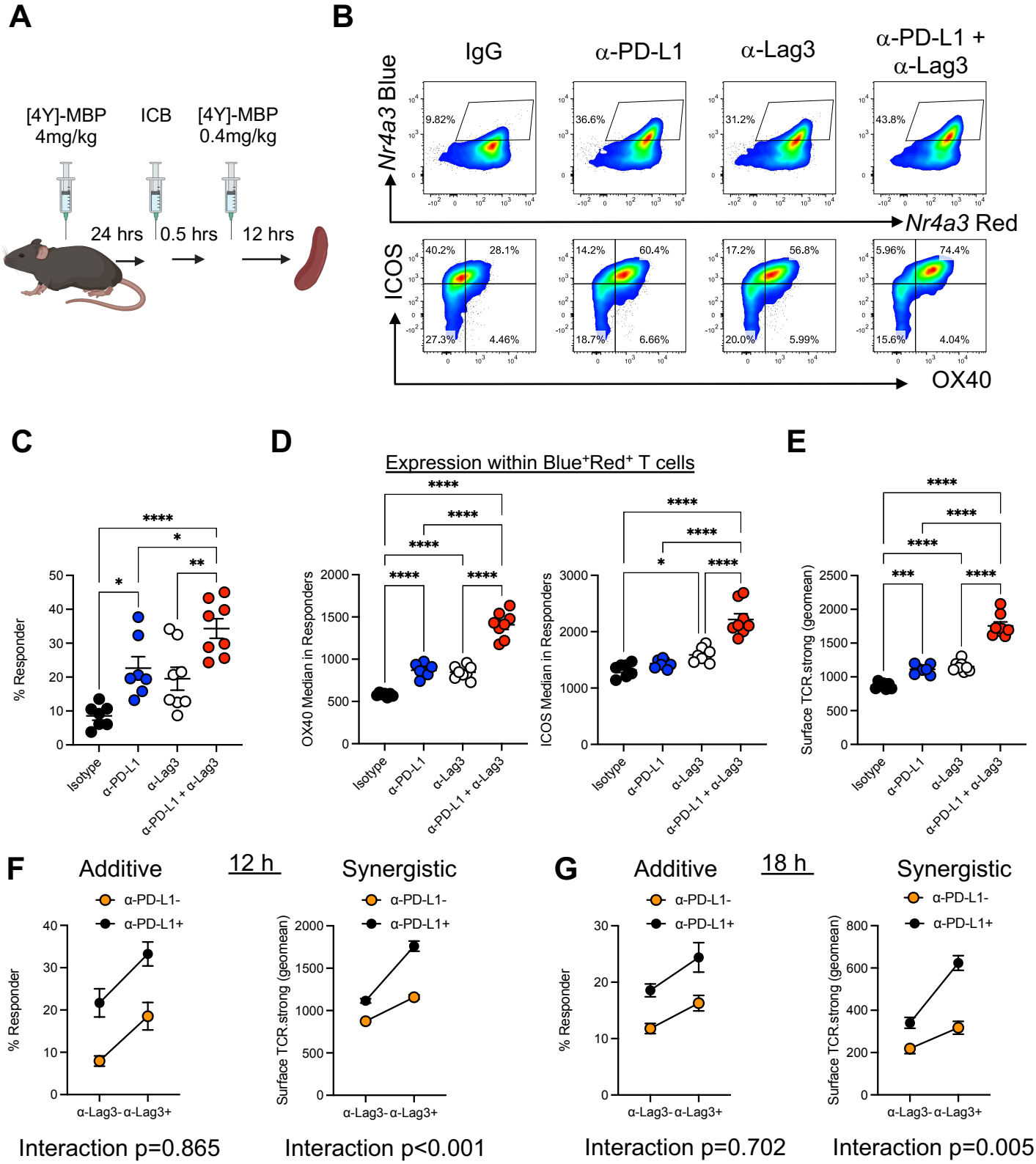
A
[4Y]-MBP 4mg/kg
ICB
[4Y]-MBP 0.4mg/kg
24 hrs
0.5 hrs
12 hrs
B
IgG
α-PD-L1
α-Lag3
α-PD-L1 + α-Lag3
Nr4a3 Blue
Nr4a3 Red
9.82%
36.6%
31.2%
43.8%
ICOS
OX40
40.2%
28.1%
27.3%
4.46%
14.2%
60.4%
18.7%
6.66%
17.2%
56.8%
20.0%
5.99%
5.96%
74.4%
15.6%
4.04%
C
% Responder
Isotype
α-PD-L1
α-Lag3
α-PD-L1 + α-Lag3
D
Expression within Blue+Red+ T cells
OX40 Median in Responders
ICOS Median in Responders
E
Surface TCR.strong (geomean)
F
12 h
Additive
Synergistic
α-PD-L1-
α-PD-L1+
α-Lag3- α-Lag3+
Interaction p=0.865
Interaction p<0.001
G
18 h
Additive
Synergistic
Interaction p=0.702
Interaction p=0.005

Figure 3

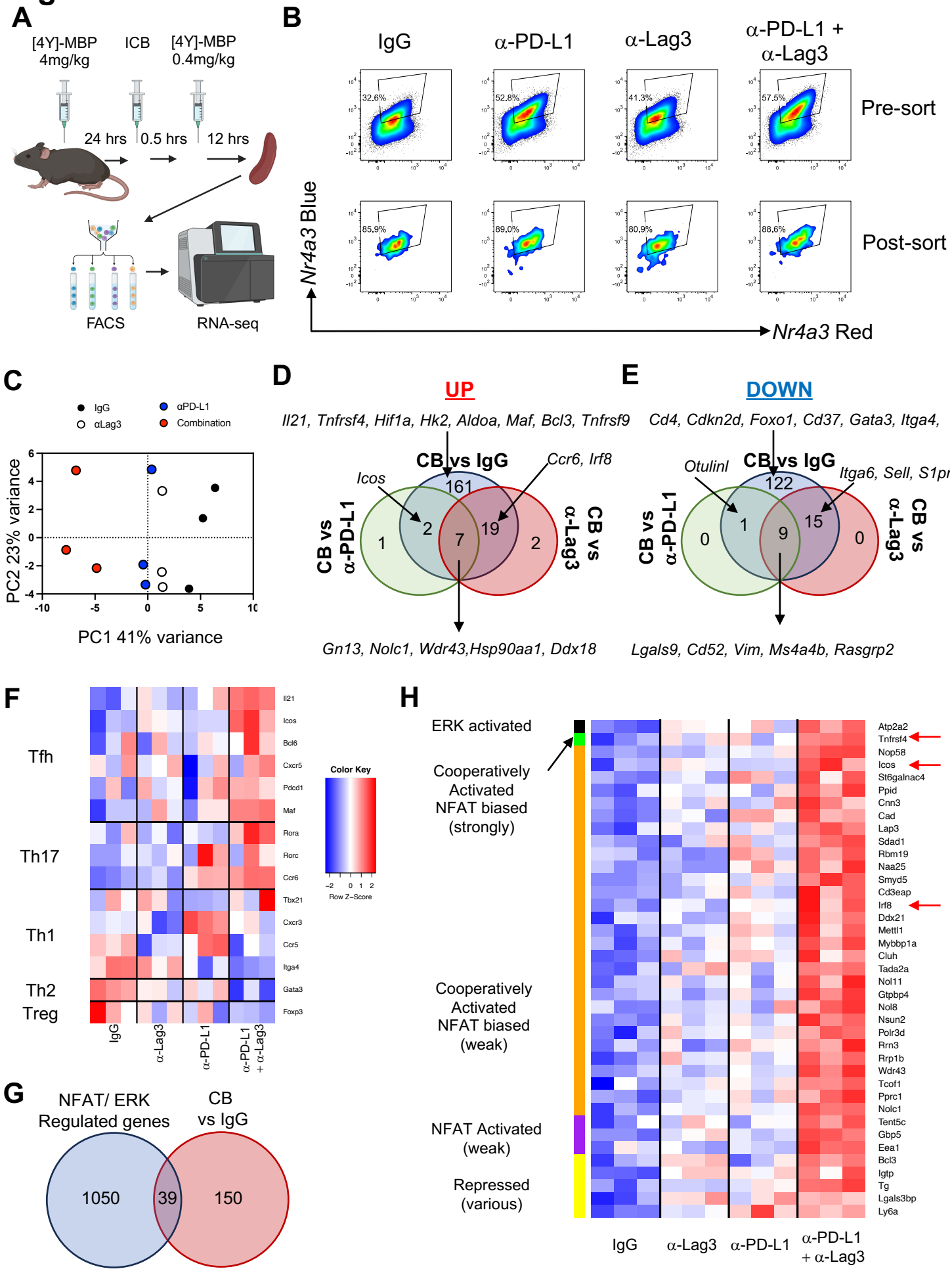
A
[4Y]-MBP 4mg/kg
ICB
[4Y]-MBP 0.4mg/kg
24 hrs
0.5 hrs
12 hrs
FACS
RNA-seq
B
IgG
α-PD-L1
α-Lag3
α-PD-L1 + α-Lag3
Pre-sort
Post-sort
32.6%
52.8%
41.3%
57.5%
85.9%
89.0%
80.9%
88.6%
Nr4a3 Blue
Nr4a3 Red
C
IgG
αLag3
αPD-L1
Combination
PC2 23% variance
PC1 41% variance
D
UP
Il21, Tnfrsf4, Hif1a, Hk2, Aldoa, Maf, Bcl3, Tnfrsf9
CB vs IgG
Icos
Ccr6, Irf8
CB vs α-PD-L1
CB vs α-Lag3
161
2
19
1
7
2
Gn13, Nolc1, Wdr43,Hsp90aa1, Ddx18
E
DOWN
Cd4, Cdkn2d, Foxo1, Cd37, Gata3, Itga4,
CB vs IgG
Otulinl
Itga6, Sell, S1pr
CB vs α-PD-L1
CB vs α-Lag3
122
1
15
0
9
0
Lgals9, Cd52, Vim, Ms4a4b, Rasgrp2
F
Tfh
Th17
Th1
Th2
Treg
Il21
Icos
Bcl6
Cxcr5
Pdcd1
Maf
Rora
Rorc
Ccr6
Tbx21
Cxcr3
Ccr5
Itga4
Gata3
Foxp3
IgG
α-Lag3
α-PD-L1
α-PD-L1 + α-Lag3
Color Key
Row Z-Score
G
NFAT/ ERK Regulated genes
CB vs IgG
1050
39
150
H
ERK activated
Cooperatively Activated NFAT biased (strongly)
Cooperatively Activated NFAT biased (weak)
NFAT Activated (weak)
Repressed (various)
Atp2a2
Tnfrsf4
Nop58
Icos
St6galnac4
Ppid
Cnn3
Cad
Lap3
Sdad1
Rbm19
Naa25
Smyd5
Cd3eap
Irf8
Ddx21
Mettl1
Mybbp1a
Cluh
Tada2a
Nol11
Gtpbp4
Nol8
Nsun2
Polr3d
Rrn3
Rrp1b
Wdr43
Tcof1
Pprc1
Nolc1
Tent5c
Gbp5
Eea1
Bcl3
Igtp
Tg
Lgals3bp
Ly6a
IgG
α-Lag3
α-PD-L1
α-PD-L1 + α-Lag3

Figure 4

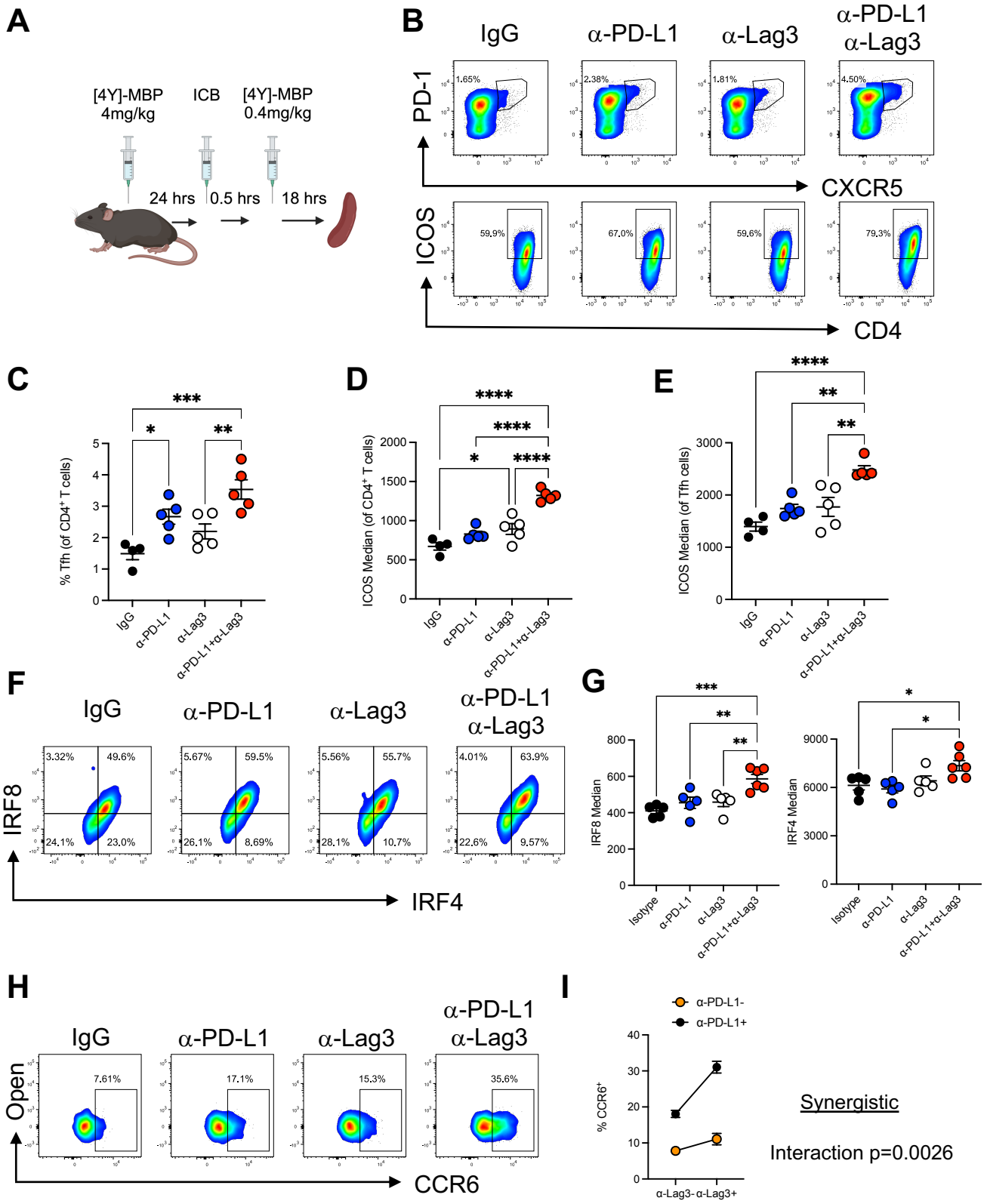
A
[4Y]-MBP
4mg/kg
ICB
[4Y]-MBP
0.4mg/kg
24 hrs
0.5 hrs
18 hrs
B
IgG
α-PD-L1
α-Lag3
α-PD-L1
α-Lag3
PD-1
CXCR5
1.65%
2.38%
1.81%
4.50%
ICOS
CD4
59.9%
67.0%
59.6%
79.3%
C
% Tfh (of CD4+ T cells)
IgG
α-PD-L1
α-Lag3
α-PD-L1+α-Lag3
D
ICOS Median (of CD4+ T cells)
E
ICOS Median (of Tfh cells)
F
IgG
α-PD-L1
α-Lag3
α-PD-L1
α-Lag3
IRF8
IRF4
3.32%
49.6%
24.1%
23.0%
5.67%
59.5%
26.1%
8.69%
5.56%
55.7%
28.1%
10.7%
4.01%
63.9%
22.6%
9.57%
G
IRF8 Median
IRF4 Median
Isotype
α-PD-L1
α-Lag3
α-PD-L1+α-Lag3
H
IgG
α-PD-L1
α-Lag3
α-PD-L1
α-Lag3
Open
CCR6
7.61%
17.1%
15.3%
35.6%
I
α-PD-L1-
α-PD-L1+
% CCR6+
α-Lag3-
α-Lag3+
Synergistic
Interaction p=0.0026

Figure 5

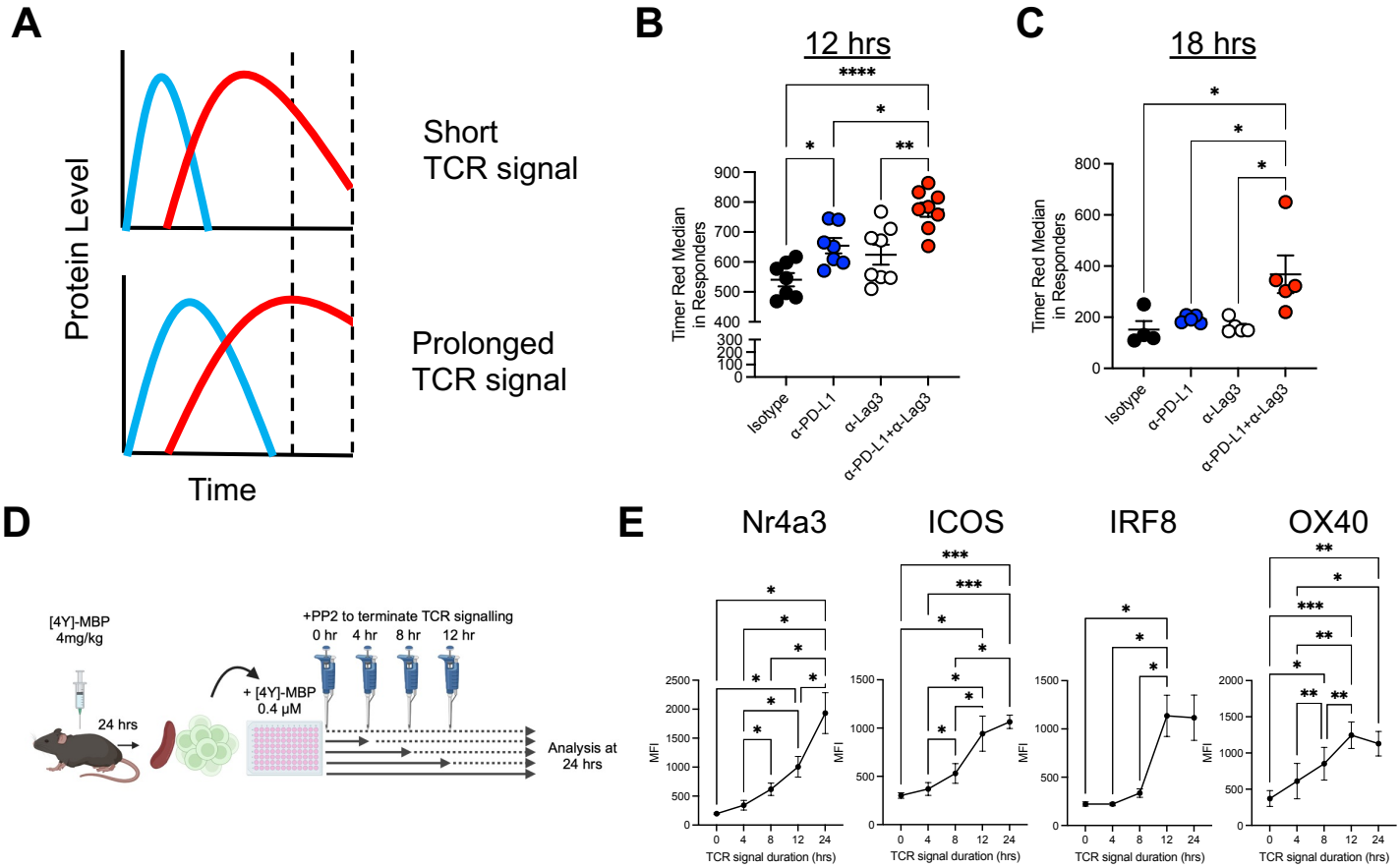
A
Protein Level
Time
Short
TCR signal
Prolonged
TCR signal
B
12 hrs
Timer Red Median
in Responders
Isotype
α-PD-L1
α-Lag3
α-PD-L1+α-Lag3
C
18 hrs
Timer Red Median
in Responders
Isotype
α-PD-L1
α-Lag3
α-PD-L1+α-Lag3
D
[4Y]-MBP
4mg/kg
24 hrs
+PP2 to terminate TCR signalling
0 hr
4 hr
8 hr
12 hr
+ [4Y]-MBP
0.4 μM
Analysis at
24 hrs
E
Nr4a3
ICOS
IRF8
OX40
MFI
TCR signal duration (hrs)

Figure 6

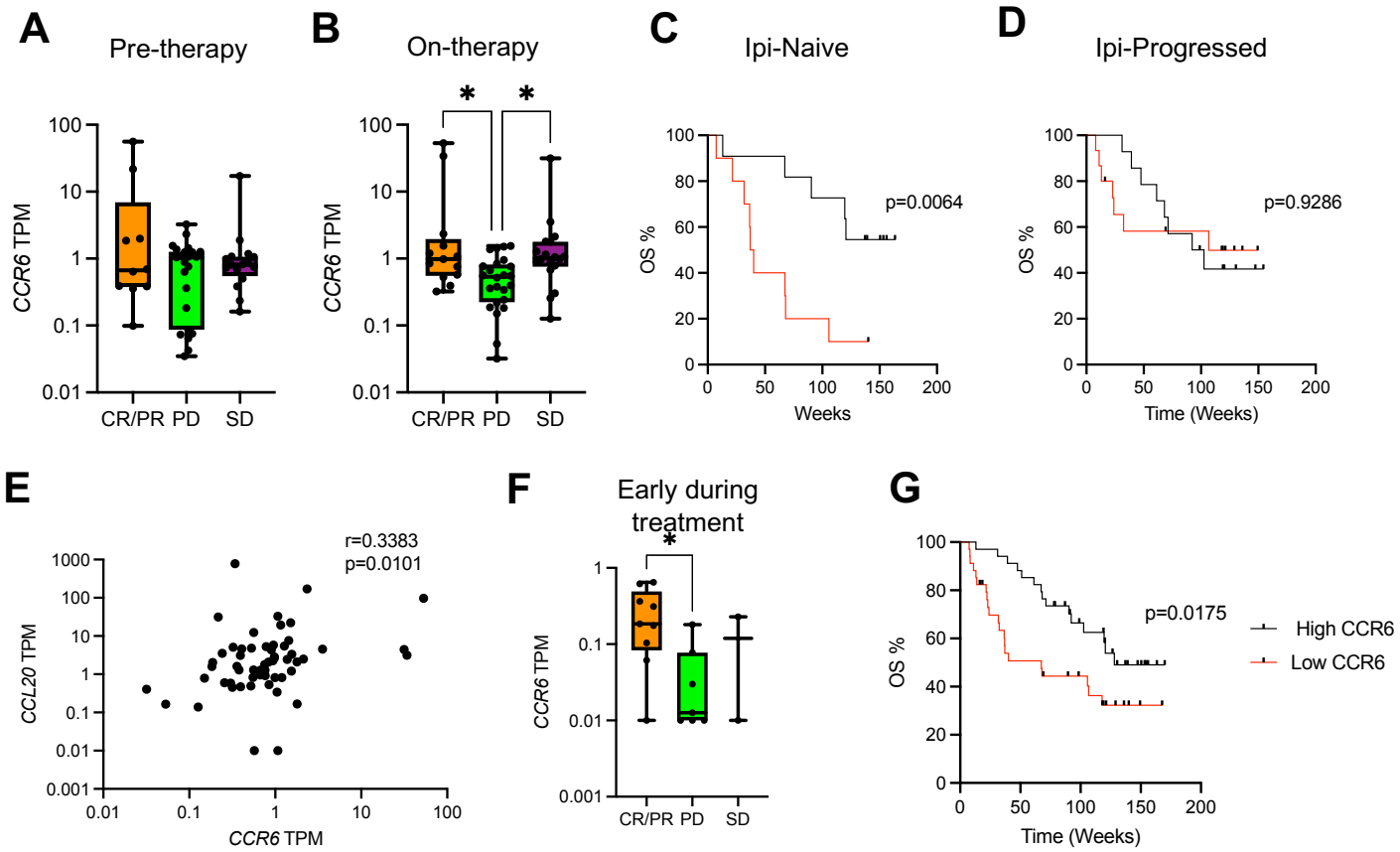
A
Pre-therapy
CCR6 TPM
100
10
1
0.1
0.01
CR/PR PD SD
B
On-therapy
*
*
CCR6 TPM
100
10
1
0.1
0.01
CR/PR PD SD
C
Ipi-Naive
OS %
p=0.0064
Weeks
D
Ipi-Progressed
OS %
p=0.9286
Time (Weeks)
E
r=0.3383
p=0.0101
CCL20 TPM
1000
100
10
1
0.1
0.01
0.001
0.01 0.1 1 10 100
CCR6 TPM
F
Early during treatment
*
CCR6 TPM
1
0.1
0.01
0.001
CR/PR PD SD
G
OS %
p=0.0175
High CCR6
Low CCR6
Time (Weeks)

Figure 7

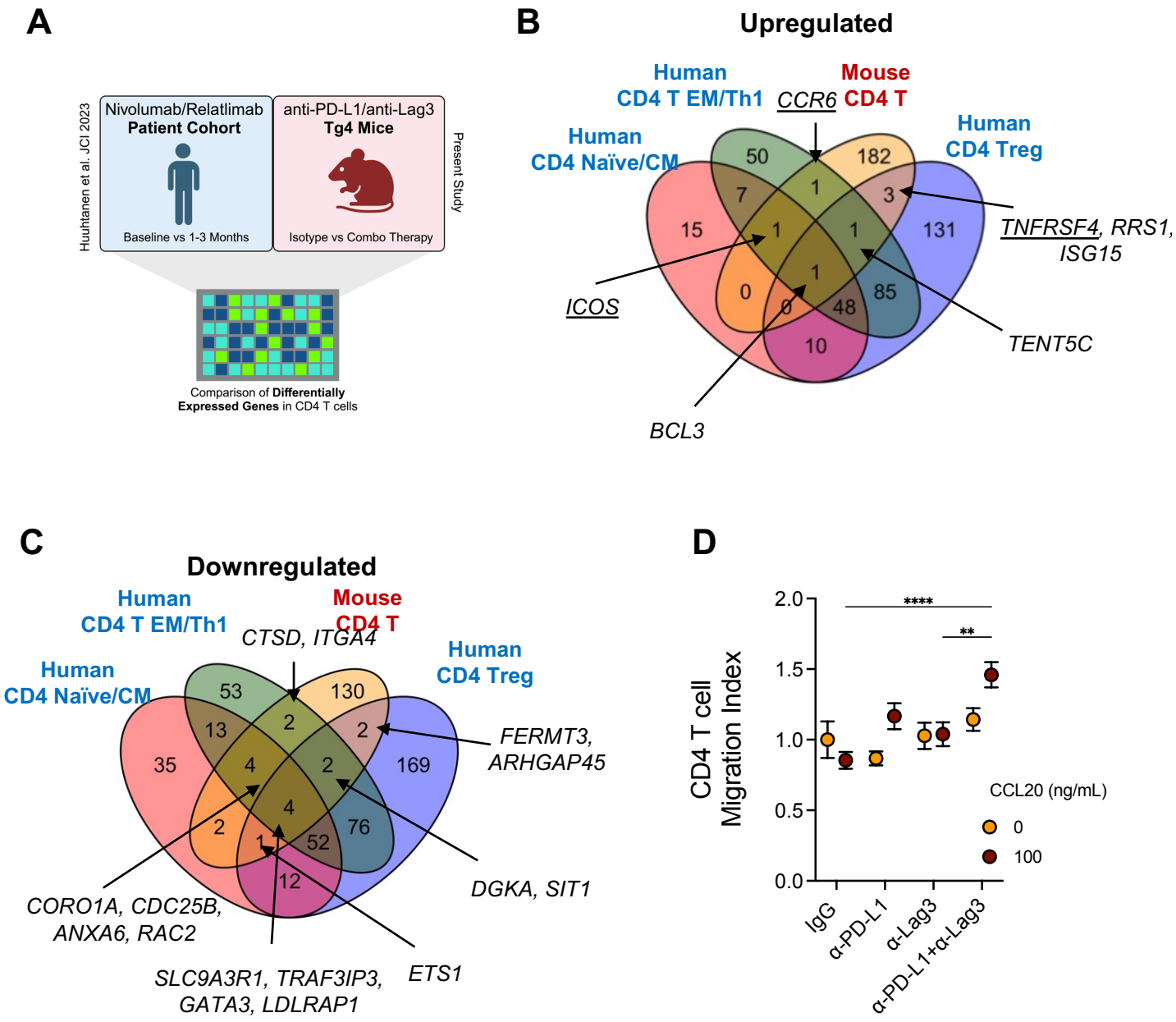
A
Huuhtanen et al. JCI 2023
Nivolumab/Relatlimab
Patient Cohort
Baseline vs 1-3 Months
anti-PD-L1/anti-Lag3
Tg4 Mice
Isotype vs Combo Therapy
Present Study
Comparison of Differentially Expressed Genes in CD4 T cells
B
Upregulated
Human CD4 T EM/Th1
Mouse CD4 T
Human CD4 Naïve/CM
Human CD4 Treg
CCR6
50
182
7
1
3
15
1
1
131
1
0
85
0
48
10
TNFRSF4, RRS1, ISG15
ICOS
TENT5C
BCL3
C
Downregulated
Human CD4 T EM/Th1
Mouse CD4 T
Human CD4 Naïve/CM
Human CD4 Treg
CTSD, ITGA4
53
130
13
2
2
35
4
2
169
4
2
76
1
52
12
FERMT3, ARHGAP45
DGKA, SIT1
CORO1A, CDC25B, ANXA6, RAC2
SLC9A3R1, TRAF3IP3, GATA3, LDLRAP1
ETS1
D
CD4 T cell Migration Index
2.0
1.5
1.0
0.5
0.0
****
**
CCL20 (ng/mL)
0
100
IgG
α-PD-L1
α-Lag3
α-PD-L1+α-Lag3